Nonlinear Dyn (2007) 48:231–252
DOI 10.1007/s11071-006-9086-0

ORIGINAL ARTICLE

Two-to-one resonant multi-modal dynamics of horizontal/inclined cables. Part I: Theoretical formulation and model validation

Narakorn Srinil · Giuseppe Rega · Somchai Chucheepsakul

Received: 21 June 2005 / Accepted: 5 May 2006 / Published online: 30 December 2006

Abstract This paper is first of the two papers dealing with analytical investigation of resonant multi-modal dynamics due to 2:1 internal resonances in the finite-amplitude free vibrations of horizontal/inclined cables. Part I deals with theoretical formulation and validation of the general cable model. Approximate nonlinear partial differential equations of 3-D coupled motion of small sagged cables – which account for both spatio-temporal variation of nonlinear dynamic tension and system asymmetry due to inclined sagged configurations – are presented. A multi-dimensional Galerkin expansion of the solution of nonplanar/planar motion is performed, yielding a complete set of system quadratic/cubic coefficients. With the aim of parametrically studying the behavior of horizontal/inclined cables in Part II [25], a second-order asymptotic analysis under planar 2:1 resonance is accomplished by the method of multiple scales. On accounting for higher-order effects of quadratic/cubic nonlinearities, approximate closed-form solutions of nonlinear amplitudes, frequencies and dynamic configurations of resonant nonlinear normal modes reveal the dependence of cable response on resonant/nonresonant modal contributions. Depending on simplifying kinematic modeling and assigned system parameters, approximate horizontal/inclined cable models are thoroughly validated by numerically evaluating statics and non-planar/planar linear/non-linear dynamics against those of the exact model. Moreover, the modal coupling role and contribution of system longitudinal dynamics are discussed for horizontal cables, showing some meaningful effects due to kinematic condensation.

Keywords Exact/approximate model · Horizontal/inclined sagged cable · Higher-order effects · Internal resonance · Longitudinal dynamics · Nonlinear free vibration

N. Srinil · G. Rega (✉)
Department of Structural and Geotechnical Engineering, University of Rome 'La Sapienza', via A. Gramsci 53, Rome 00197, Italy
e-mail: giuseppe.rega@uniromal.it

S. Chucheepsakul
Department of Civil Engineering, King Mongkut's University of Technology Thonburi, Bangmod, Bangkok 10140, Thailand

1 Introduction

Internally resonant nonlinear dynamics due to finite vibration amplitudes of elastic suspended cables have received a considerable amount of attention over the years, as they exhibit a variety of extraordinarily rich phenomena induced by the overall structural high-flexibility and low-damping characteristics. Depending on the values of some geometrical/mechanical control parameters and on system frequencies, the activated internal resonances enhance modal coupling capacity, even in the absence of external excitations.

A comprehensive account of internal resonance mechanisms in suspended cables can be found in a recent updated review on cable nonlinear dynamics [1, 2].

Suspended cables exhibit various planar (e.g., 2:1, 3:1, 1:1) and nonplanar (e.g., 2:1, 1:1) internal resonance conditions due to the inherent combination of system quadratic and cubic nonlinearities [3]. The system, involving different interacting planar/nonplanar modes in the response, may, in turn, experience a multiple internal resonance [2, 4]. The richness of cable nonlinear dynamics due to single [5–7] or multiple [8–12] internal resonances has been highlighted by a large number of theoretical, numerical, and/or experimental studies based on low- or multi-dimensional models. While most works deal with resonant horizontal cables, usually at the so-called first crossover in the natural frequency spectrum [13], few have been devoted to resonant inclined cables exhibiting the system asymmetry due to actual inclined configurations [14]. Some studies involving other non-crossover resonant horizontal cables have also been carried out [3, 15]. As to the theoretical modeling, the following main situations – particularly those worth easing the analytical computations – have been addressed:

(i) Parabolic (i.e., shallow) horizontal or nearly taut inclined [16–18] cables exhibiting either symmetric or anti-symmetric modal shapes.
(ii) Kinematically condensed cable model exhibiting space-independent dynamic tension, in which the governing integro-partial differential equations of motion ensue from neglecting the longitudinal inertia according to a quasi-static stretching assumption of cable in motion and linking the longitudinal displacement field to the transversal ones.
(iii) Low finite-dimensional models of system ordinary differential equations (ODEs) obtained by expanding the dynamic displacement fields in terms of some eigenfunctions, e.g., usually, of the solely resonant modes, via a Galerkin-based approximation.

To overcome some of the aforementioned issues, either analytical/numerical [19] or purely numerical [20, 21] approaches have been used for investigating some important aspects of the response of non-condensed, multi-dimensional, arbitrarily sagged, or inclined cables whose theoretical formulation relies on exact kinematic modeling. Alternatively, refined analytical techniques – still applied to the parabolic condensed horizontal cable – have been proposed to improve the (iii) issue. They consist of applying the method of multiple scales (MMS) either directly to the original PDEs without a priori assumptions of the displacement solution form [11, 12, 22, 23], or to the discretized model accounting for the full-basis eigenspectrum of linear modes in the Galerkin projection of the PDEs [23]. As a matter of fact, the outcomes of the latter technique are substantially equivalent to those provided by the former, if enough modes are retained in the discretization [24].

The present work in two parts still fits in an analytical framework, which is deemed capable of enlightening the fundamental features of system nonlinear dynamics, while also establishing a link between analytical and numerical treatments, the prediction of the former being observed against some outcomes of the latter. Accordingly, Part I presents and compares exact and approximate models of a general, non-condensed, arbitrarily inclined cable, as well as the discretization-type perturbation analysis of the approximate model, to be subsequently used in Part II [25] for investigating the nonlinear free vibrations of horizontal/inclined cables due to 2:1 internal resonances. Nonlinear free vibrations have mostly been studied by considering a condensed horizontal cable, with only one or two degrees-of-freedom (DOF) [26–29]. The non-condensed horizontal/inclined cable model with three DOF has been considered in [30]. Yet, the significant role played by internal resonances has been overlooked in all of these studies. Recently, the basic (i.e., 2:1, 3:1, 1:1) internal resonances of a still condensed horizontal cable have been addressed [3] based on a general analytical formulation [23]. Herein, attention is focused on 2:1 resonances because, besides discriminating a typical dynamic scenario between horizontal and inclined cables, it is the solely resonance where it makes sense to develop a higher-order asymptotic analysis accounting for contributions from all of resonant/nonresonant modes due to system quadratic nonlinearities.

The paper is organized as follows. In Section 2, the nonlinear PDEs of 3-D motion accounting for both dynamic tension space–time variation and system asymmetry due to inclined sagged configurations are presented for exact/approximate cable models. Closed-form static and linear dynamic solutions of small-sagged cables are summarized. An infinite-dimensional Galerkin expansion of the solution of approximate

PDEs is presented in Section 3, wherein the effects of neglecting the system longitudinal inertia are also evidenced. For planar 2:1 internal resonances, a second-order asymptotic analysis is accomplished through the MMS in Section 4, accounting for higher-order effects of quadratic/cubic nonlinearities. Approximate nonlinear solutions of resonant amplitudes, frequencies, space–time displacement, and velocity fields associated with the nonlinear normal modes are determined, highlighting the dependence of cable response on different resonant/nonresonant modes. In Section 5, the approximate static, nonplanar/planar linear and nonlinear dynamic results of horizontal/inclined cables are thoroughly validated against those of the exact model, and the role played by the system longitudinal dynamics is discussed, along with some observed effects due to kinematic condensation. The outcomes allow for a proper approximate model selection. The concluding remarks are drawn in Section 6.

2 Cable model and governing equations

Figure 1 displays a suspended cable with arbitrary inclination angle θ in a fixed Cartesian coordinate (X, Y, Z) system. Three different configurations of the infinitesimal cable element in the natural (ds_{n}), static (ds), and dynamic (final, ds_{f}) states are considered for the exact model, whereas for the approximate model it is usually assumed $ds \approx ds_{\mathrm{n}}$. The function $y = y(x)$ describes the cable planar static equilibrium under gravity g. While keeping the horizontal span X_H fixed, the vertical span Y_H is varied to attain specified θ values. The relevant in-plane (out-of-plane) dynamics is described by the longitudinal or horizontal u and vertical $v(w)$ displacements measured from the static configuration. Here, x is the spatially independent variable, and t denotes time. A prime (overdot) denotes differentiation with respect to $x(t)$.

2.1 Exact equations of motion

In the absence of damping and external loading, a perfectly flexible, linear elastic cable with negligible torsional, bending and shear rigidities is considered, with the strain energy being only due to cable axial stretching. Based on the so-called engineering strain measure, the exact kinematic modeling of the total strain of cable element is given by

$$e_{\mathrm{f}} = \frac{ds_{\mathrm{f}}}{ds_{\mathrm{n}}} - 1 = \frac{1+e}{\sqrt{1+y'^2}}\sqrt{(1+u')^2 + (y'+v')^2 + w'^2} - 1, \quad (1)$$

where $e = (ds - ds_{\mathrm{n}})/ds_{\mathrm{n}}$ is the initial static strain. By means of the variational formulation, the governing exact PDEs of 3-D coupled undamped unforced motion

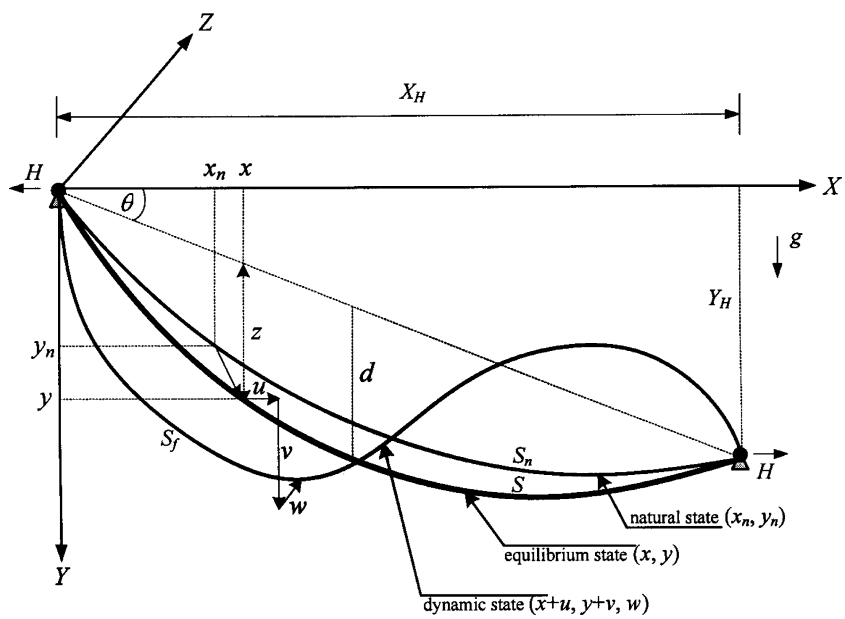

Fig. 1 Configurations of an inclined cable

of the cable about its static equilibrium read [20, 21, 31]:

$$\left(\frac{EA+EA(1+e)u'}{\sqrt{1+y'^2}}-\frac{EA\left(1+u'\right)}{\sqrt{(1+u')^2+(y'+v')^2+w'^2}}\right)' = \frac{w_C\sqrt{1+y'^2}}{g(1+e)}\ddot{u}, \tag{2}$$

$$\left(\frac{EAy'+EA(1+e)v'}{\sqrt{1+y'^2}}-\frac{EA\left(y'+v'\right)}{\sqrt{(1+u')^2+(y'+v')^2+w'^2}}\right)' = \frac{w_C\sqrt{1+y'^2}}{g(1+e)}\ddot{v}, \tag{3}$$

$$\left(\frac{EA(1+e)w'}{\sqrt{1+y'^2}}-\frac{EAw'}{\sqrt{(1+u')^2+(y'+v')^2+w'^2}}\right)' = \frac{w_C\sqrt{1+y'^2}}{g(1+e)}\ddot{w}, \tag{4}$$

in which zero values of static and dynamic displacements of the boundaries are considered. E is the Young's modulus, w_C the cable self-weight per unit unstretched length, and A its uniform cross-sectional area. This system is highly nonlinear and its closed-form analytical solution cannot be sought. Hence, either a direct numerical [14, 21] or an approximate analytical solution based on some assumptions has to be pursued.

2.2 Approximate equations of motion

In conditions of moderately large vibration amplitudes, the radical term in Equation (1) is expanded through the binomial series by discarding the higher-order effects. Along with the assumption of small initial strain ($ds \approx ds_n$), i.e., $1+e \approx 1$, Equation (1) becomes

$$e_f = e + e_d \approx e + \frac{1}{1+y'^2}\left(u' + y'v' + \frac{1}{2}(u'^2+v'^2+w'^2)\right), \tag{5}$$

where the extensional dynamic strain e_d is expressed through its Lagrangian measure. For convenience in the parametric analysis, the dimensionless variables,

$$\tilde{x} = \frac{x}{X_H}, \quad \tilde{y} = \frac{y}{X_H}, \quad \tilde{u} = \frac{u}{X_H}, \quad \tilde{v} = \frac{v}{X_H}, \quad \tilde{w} = \frac{w}{X_H}, \quad \alpha = \frac{EA}{H}, \quad \tilde{t} = \frac{t}{X_H}\sqrt{\frac{gH}{w_C}}, \tag{6}$$

are introduced, in which H is the horizontal component of cable static tension. The approximate, third-order, nonlinear PDEs, valid for both horizontal and arbitrarily inclined cables, are given, in non-dimensional form, by

$$\rho\ddot{u} = \left\{u' + \frac{\alpha}{\rho^3}(u'+y'v') + \frac{\alpha}{\rho^3}\left(u'^2+y'u'v'+\frac{1}{2}(u'^2+v'^2+w'^2)\right) + \frac{\alpha}{2\rho^3}(u'^3+u'v'^2+u'w'^2)\right\}', \tag{7}$$

$$\rho\ddot{v} = \left\{v' + \frac{\alpha}{\rho^3}(y'u'+y'^2v') + \frac{\alpha}{\rho^3}\left(u'v'+y'v'^2+\frac{y'}{2}(u'^2+v'^2+w'^2)\right) + \frac{\alpha}{2\rho^3}(u'^2v'+v'^3+v'w'^2)\right\}', \tag{8}$$

$$\rho\ddot{w} = \left\{w' + \frac{\alpha}{\rho^3}(u'w'+y'v'w') + \frac{\alpha}{2\rho^3}(w'u'^2+w'v'^2+w'^3)\right\}', \tag{9}$$

where $\rho = \sqrt{1+y'^2}$. The $(\sim)$ notation has been dropped for brevity, and the corresponding homogeneous boundary conditions (b.c.) are $u(0,t) = u(1,t) = v(0,t) = v(1,t) = w(0,t) = w(1,t) = 0$. Apart from damping and external forces, sets of equations similar to (7)–(9), based on the Lagrangian strain measure, have been previously reported in the literature [e.g., 28, 30, 32–34] yet with few (typo) errors found in some references. However, in contrast with the so-called kinematically condensed model (see Appendix A), herein (i) the second-order term of the longitudinal displacement gradient u'^2 and (ii) the corresponding inertia $\ddot{u}$ are kept in the formulation. Moreover, (iii) Equations (7)–(9) exhibit

both quadratic and cubic nonlinear effects due to cable stretching, the former occurring even in the absence of initial sag or curvature (taut string case). Thus, the dynamic strain in Equation (5) turns out to be spatially nonuniform.

2.3 General closed-form static solution

Based on Fig. 1, wherein $y = x\tan\theta + z$, and Equation (6), with $\tilde{z} = z/X_H$, the approximate nonlinear equation governing the vertical static equilibrium of the inclined cable, with the omitted ($\sim$), is given by [14]

$$\frac{Hz''}{X_H} = -w_C(1 + (\tan\theta + z')^2)^{1/2}. \tag{10}$$

Following [13], in which z' is considered sufficiently small for its square to be neglected according to the small sag assumption, the approximate static solution can be expressed, up to cubic order of x, as

$$Z \approx \frac{1}{2}x(1-x)\left(1 + \frac{\varepsilon*}{6}(1-2x)\right) + O(\varepsilon*^2), \tag{11}$$

with $Z = z/(w_C X_H \sec\theta/H)$ and $\varepsilon* = w_C X_H \sin\theta/H$ being non-dimensional parameters. Equation (11) is valid as $\varepsilon*$ is small when the inclined cable has a small sag-to-span ratio. It is also valid for horizontal cables, where $\varepsilon* = 0$ as $\theta = 0$. Because one may assume $ds \approx dx$ for shallow cables, being $\rho \approx 1$ in the static analysis entails $H \approx w_C X_H/8d$, in which d is the cable sag-to-span ratio (being 1:8 or less [13]). Accordingly, Equation (11) renders $y = z \approx 4dx(1-x)$, which is the parabolic configuration. In contrast, by accounting for the asymmetry effect to the first order of $\varepsilon*$, the inclined profile is no longer parabolic (symmetric) [35] as typically considered in the literature on nonlinear dynamics of inclined cables, e.g. [16–18, 34].

2.4 Natural frequencies and mode shapes

The in-plane and out-of-plane displacements are postulated in the form:

$$U^J(x,t) = \sum_{n=1}^{N} D_n^J(t)\,\Phi_n(x), \tag{12}$$

where, for $J = 1$ to 3, $U^1 = u$, $U^2 = v$ and $U^3 = w$, $\Phi_n(x) = \sin(n\pi x)$, N being the number of retained terms in the sine series. Substituting Equation (12) into Equations (7)–(9), neglecting nonlinear terms and applying the Galerkin method with b.c., a set of $3N$ coupled ODEs for the generalized time co-ordinates D_n^J is obtained in the following general matrix form:

$$\begin{aligned}
&[\bar{M}]\{\ddot{\bar{D}}\} + [\bar{K}]\{\bar{D}\} = 0,\\
&\{\bar{D}\} = \left\{\begin{array}{l} \lfloor D_1^1, D_2^1, \ldots, D_N^1\rfloor^{\mathrm{T}} \\ \lfloor D_1^2, D_2^2, \ldots, D_N^2\rfloor^{\mathrm{T}} \\ \lfloor D_1^3, D_2^3, \ldots, D_N^3\rfloor^{\mathrm{T}} \end{array}\right\},\\
&[\bar{M}] = \begin{bmatrix} [\bar{M}_{uu}] & 0 & 0 \\ 0 & [\bar{M}_{vv}] & 0 \\ 0 & 0 & [\bar{M}_{ww}] \end{bmatrix},\\
&[\bar{K}] = \begin{bmatrix} [\bar{K}_{uu}] & [\bar{K}_{uv}] & 0 \\ [\bar{K}_{uv}] & [\bar{K}_{vv}] & 0 \\ 0 & 0 & [\bar{K}_{ww}] \end{bmatrix}.
\end{aligned} \tag{13}$$

The components in the $N \times N$ sub-mass and sub-stiffness matrices of $[\bar{M}]$ and $[\bar{K}]$ which depend on the static solution variables are:

$$\begin{aligned}
m_{uu}(n,m) &= m_{vv}(n,m) = m_{ww}(n,m)\\
&= \int_0^1 \rho\Phi_n\Phi_m dx,\\
k_{uu}(n,m) &= \int_0^1 \Phi_n'\left(1 + \frac{\alpha}{\rho^3}\right)\Phi_m' dx,\\
k_{uv}(n,m) &= \int_0^1 \Phi_n'\left(\frac{\alpha y'}{\rho^3}\right)\Phi_m' dx = k_{vu}(n,m),\\
k_{vv}(n,m) &= \int_0^1 \Phi_n'\left(1 + \frac{\alpha y'^2}{\rho^3}\right)\Phi_m' dx,\\
k_{ww}(n,m) &= \int_0^1 \Phi_n'\Phi_m' dx,
\end{aligned} \tag{14}$$

for $n, m = 1, 2, \ldots, N$. For horizontal cables, consistent with the static parabolic assumption, $\rho \approx 1$ in Equation (14); otherwise, $\rho \neq 1$ for inclined cables. The dimensionless frequency is $\omega = \bar{\omega} X_H\sqrt{w_C/gH}$, and the corresponding modal shapes are obtained through Equation (12), upon numerical integration of (13). In turn, linear dynamic solutions of vertical and out-of-plane motion of the condensed horizontal cable are known in closed form (see Appendix A).

3 Multi-mode discretization for nonlinear dynamics

To deal with the nonlinear dynamic problem, Equations (7)–(9) are first cast in state-space (first-order) form. Accounting for the orthonormality properties of linear eigenmodes, these equations are projected onto the system full eigenbasis by letting

$$U^J(x,t)=\sum_{m=1}^{\infty} f_m(t)\zeta_m^J(x),$$
$$V^J(x,t)=\sum_{m=1}^{\infty} p_m(t)\zeta_m^J(x), \tag{15}$$
$$w(x,t)=\sum_{n=1}^{\infty} h_n(t)\xi_n(x),$$
$$\dot{w}(x,t)=\sum_{n=1}^{\infty} q_n(t)\xi_n(x), \tag{16}$$

where now $J=1$–2, $U^1=u$, $U^2=v$, $V^1=\dot{u}$, $V^2=\dot{v}$, $\zeta_m^1=\phi_m$, $\zeta_m^2=\varphi_m$, f_m and p_m (h_n and q_n) being the displacement and velocity modal coordinates associated with both the longitudinal ϕ_m and vertical φ_m (out-of-plane ξ_n) shape functions of the m in-plane (n out-of-plane) mode. Then, the Galerkin method is applied to the first-order equations, using (15), (16) and the b.c., thereby yielding the infinite set of coupled ODEs of in-plane and out-of-plane co-ordinates as:

$$\dot{f}_m - p_m = 0, \tag{17a}$$
$$\dot{p}_m+\omega_m^2 f_m=\sum_{i=1}^{\infty}\sum_{j=1}^{\infty}\Lambda_{mij}f_i f_j+\sum_{i=1}^{\infty}\sum_{j=1}^{\infty}\vartheta_{mij}h_i h_j+\sum_{i=1}^{\infty}\sum_{j=1}^{\infty}\sum_{k=1}^{\infty}\Gamma_{mijk}f_i f_j f_k+\sum_{i=1}^{\infty}\sum_{j=1}^{\infty}\sum_{k=1}^{\infty}\Upsilon_{mijk}f_i h_j h_k, \tag{17b}$$
$$\dot{h}_n - q_n = 0, \tag{18a}$$
$$\dot{q}_n+\omega_n^2 h_n=\sum_{i=1}^{\infty}\sum_{j=1}^{\infty}\Psi_{nij}h_i f_j+\sum_{i=1}^{\infty}\sum_{j=1}^{\infty}\sum_{k=1}^{\infty}\Theta_{nijk}h_i h_j h_k+\sum_{i=1}^{\infty}\sum_{j=1}^{\infty}\sum_{k=1}^{\infty}\Delta_{nijk}h_i f_j f_k, \tag{18b}$$

for $\forall m,n=1,\ldots,+\infty$, where ω_m (ω_n) are the in-plane (out-of-plane) natural frequencies. This general system describes the nonlinear temporal problem for a non-condensed or condensed cable model. Depending on the element kinematic modeling, the pertinent quadratic and cubic nonlinear coefficients are different, as comparatively given as follows.

(i) For non-condensed model of horizontal/inclined cables,

$$\Lambda_{mij}=-\int_0^1\frac{\alpha}{\rho^3}\left\{\phi_m'\left(\frac{3}{2}\phi_i'\phi_j'+y'\phi_i'\varphi_j'+\frac{1}{2}\varphi_i'\varphi_j'\right)+\varphi_m'\left(\frac{y'}{2}\phi_i'\phi_j'+\phi_i'\varphi_j'+\frac{3}{2}y'\varphi_i'\varphi_j'\right)\right\}dx, \tag{19a}$$
$$\vartheta_{mij}=-\int_0^1\frac{\alpha}{2\rho^3}(\phi_m'\xi_i'\xi_j'+y'\varphi_m'\xi_i'\xi_j')dx, \tag{19b}$$
$$\Psi_{nij}=-\int_0^1\frac{\alpha}{\rho^3}\xi_n'(\xi_i'\phi_j'+y'\xi_i'\varphi_j')dx, \tag{19c}$$
$$\Gamma_{mijk}=-\int_0^1\frac{\alpha}{2\rho^3}\left\{\phi_m'(\phi_i'\phi_j'\phi_k'+\phi_i'\varphi_j'\varphi_k')+\varphi_m'(\phi_i'\phi_j'\varphi_k'+\varphi_i'\varphi_j'\varphi_k')\right\}dx, \tag{19d}$$
$$\Upsilon_{mijk}=-\int_0^1\frac{\alpha}{2\rho^3}(\phi_m'\phi_i'\xi_j'\xi_k'+\varphi_m'\varphi_i'\xi_j'\xi_k')dx, \tag{19e}$$
$$\Theta_{nijk}=-\int_0^1\frac{\alpha}{2\rho^3}\xi_n'\xi_i'\xi_j'\xi_k'\,dx, \tag{19f}$$
$$\Delta_{nijk}=-\int_0^1\frac{\alpha}{2\rho^3}\xi_n'(\xi_i'\phi_j'\phi_k'+\xi_i'\varphi_j'\varphi_k')dx. \tag{19g}$$

(ii) For condensed model of horizontal cables,

$$\Lambda_{mij}=\alpha\left\{\int_0^1\varphi_m\varphi_i''dx\int_0^1 y'\varphi_j'dx+\frac{1}{2}\int_0^1\varphi_m y''dx\int_0^1\varphi_i'\varphi_j'dx\right\}, \tag{20a}$$

$$\vartheta_{mij} = \frac{\alpha}{2}\left\{\int_0^1 \varphi_m y'' dx \int_0^1 \xi_i' \xi_j' dx\right\}, \tag{20b}$$

$$\Psi_{nij} = \alpha\left\{\int_0^1 \xi_n \xi_i'' dx \int_0^1 y' \varphi_j' dx\right\}, \tag{20c}$$

$$\Gamma_{mijk} = \frac{\alpha}{2}\left\{\int_0^1 \varphi_m \varphi_i'' dx \int_0^1 \varphi_j' \varphi_k' dx\right\}, \tag{20d}$$

$$\Upsilon_{mijk} = \frac{\alpha}{2}\left\{\int_0^1 \varphi_m \varphi_i'' dx \int_0^1 \xi_j' \xi_k' dx\right\}, \tag{20e}$$

$$\Theta_{nijk} = \frac{\alpha}{2}\left\{\int_0^1 \xi_n \xi_i'' dx \int_0^1 \xi_j' \xi_k' dx\right\}, \tag{20f}$$

$$\Delta_{nijk} = \frac{\alpha}{2}\left\{\int_0^1 \xi_n \xi_i'' dx \int_0^1 \varphi_j' \varphi_k' dx\right\}. \tag{20g}$$

Contrary to Equation (20), where the longitudinal displacement effects are solely accounted for through the independent vertical eigenfunctions φ (for horizontal cables), they are explicitly captured in Equation (19), which, in addition, accounts for also the geometrical effects of the ρ^3-term. Generally speaking, the kinematic condensation entails approximate products of integrals of the shape functions, in lieu of the exact integrals of their products provided by the non-condensed model. Depending on cable static solutions and eigenfunctions, the effects of disregarding the ρ^3-term (i.e., by setting $\rho \approx 1$) on nonlinear dynamics and the contributions of longitudinal displacement to the non-condensed coefficients will be discussed in Sections 5.3 and 5.4, respectively, along with some points on kinematic condensation effects.

4 Multiple scales analysis

Emphasis is placed on the theoretical treatment of a planar 2:1 resonance. The motivation is twofold. (i) The main differences between the nonlinear dynamics of horizontal/inclined cables are concerned with planar dynamics [20]. (ii) The 2:1 resonance is the only one which allows for highlighting higher-order effects of the quadratic nonlinearities on system dynamics, to be captured within a MMS analysis through a second-order uniform expansion [23] of the asymptotic solution of Equation (17), with no out-of-plane terms.

4.1 Second-order asymptotic solution

With ε denoting a small, non-dimensional, bookkeeping parameter of the order of amplitude of the solution, the generalized co-ordinates of displacement and velocity are sought as

$$f_m(t;\varepsilon) \approx \sum_{k=1}^{3} \varepsilon^k f_{mk}(T_0, T_1, T_2),$$
$$p_m(t;\varepsilon) \approx \sum_{k=1}^{3} \varepsilon^k p_{mk}(T_0, T_1, T_2) \tag{21}$$

where $T_0 = t$, $T_1 = \varepsilon t$ and $T_2 = \varepsilon^2 t$, the latter two time scales characterizing the slow modulation in amplitudes and phases due to nonlinearity and modal coupling effects. The first derivative with respect to t is given by $\partial/\partial t = D_0 + \varepsilon D_1 + \varepsilon^2 D_2 + \cdots$, where $D_n = \partial/\partial T_n$. Substituting Equation (21) into (17), using the independence property of the time scales and equating coefficients of like powers of ε leads to

$$\varepsilon\colon D_0 f_{m1} - p_{m1} = 0, \quad D_0 p_{m1} + \omega_m^2 f_{m1} = 0. \tag{22}$$

$$\varepsilon^2\colon D_0 f_{m2} - p_{m2} = -D_1 f_{m1},$$
$$D_0 p_{m2} + \omega_m^2 f_{m2} = -D_1 p_{m1} + \sum_{i=1}^{\infty}\sum_{j=1}^{\infty} \Lambda_{mij} f_{i1} f_{j1}. \tag{23}$$

$$\varepsilon^3\colon D_0 f_{m3} - p_{m3} = -D_1 f_{m2} - D_2 f_{m1},$$
$$D_0 p_{m3} + \omega_m^2 f_{m3} = -D_1 p_{m2} - D_2 p_{m1} + \sum_{i=1}^{\infty}\sum_{j=1}^{\infty} \Lambda_{mij}(f_{i1} f_{j2} + f_{i2} f_{j1}) + \sum_{i=1}^{\infty}\sum_{j=1}^{\infty}\sum_{k=1}^{\infty} \Gamma_{mijk} f_{i1} f_{j1} f_{k1}. \tag{24}$$

for $\forall m = 1, 2, \ldots, +\infty$. The nearness of the two (r, s) in-plane frequencies involved in a 2:1 internal resonance is described by introducing an internal detuning parameter σ such that $\omega_s = 2\omega_r + \varepsilon\sigma$. Because the governing equations at orders ε, ε^2, and ε^3 are identical to those given in [23], with the differences being only in the condensed/non-condensed coefficients, the same line of MMS analysis is herein pursued and summarized. By accounting for the interaction of two coupled

modes, the ε-order solutions of Equation (22) are taken as

$$f_{m1} = A_m(T_1, T_2)\, e^{\mathrm{i}\omega_m T_0}(\delta_{mr} + \delta_{ms}) + \mathrm{cc}, \tag{25a}$$

$$p_{m1} = \mathrm{i}\omega_m A_m(T_1, T_2)\, e^{\mathrm{i}\omega_m T_0}(\delta_{mr} + \delta_{ms}) + \mathrm{cc}, \tag{25b}$$

where A_m are complex amplitudes, $i = \sqrt{-1}$, cc denotes the complex conjugate of the preceding terms and δ_{ms}, δ_{ns} are Kronecker deltas. Substituting Equation (25) into (23) leads to

$$D_0 f_{m2} - p_{m2} = -(D_1 A_m)\, e^{\mathrm{i}\omega_m T_0}(\delta_{mr} + \delta_{ms}) + cc, \tag{26}$$

$$\begin{aligned} D_0 p_{m2} + \omega_m^2 f_{m2} = {} & -\mathrm{i}\omega_m (D_1 A_m)\, e^{\mathrm{i}\omega_m T_0}(\delta_{mr} + \delta_{ms}) \\ & + \Lambda_{mrr}\left(A_r^2 e^{2\mathrm{i}\omega_r T_0} + A_r \bar{A}_r\right) \\ & + \Lambda_{mss}\left(A_s^2 e^{2\mathrm{i}\omega_s T_0} + A_s \bar{A}_s\right) \\ & + (\Lambda_{mrs} + \Lambda_{msr})\, A_r A_s e^{\mathrm{i}(\omega_r + \omega_s)T_0} \\ & + (\Lambda_{mrs} + \Lambda_{msr})\, A_s \bar{A}_r e^{\mathrm{i}(\omega_s - \omega_r)T_0} \\ & + cc, \end{aligned} \tag{27}$$

where $\bar{A}_m$ denotes the complex conjugate of A_m. When $m = r$ or $m = s$, the particular solutions of Equations (26) and (27) contain secular effects generated by the first term on the relevant right-hand sides and by the internally resonant small-divisor terms. These effects are eliminated by enforcing the solvability conditions

$$2\mathrm{i}\omega_r (D_1 A_r) = (\Lambda_{rrs} + \Lambda_{rsr})\, A_s \bar{A}_r e^{\mathrm{i}\sigma T_1}, \tag{28a}$$

$$2\mathrm{i}\omega_s (D_1 A_s) = \Lambda_{srr} A_r^2 e^{-\mathrm{i}\sigma T_1}. \tag{28b}$$

Solving these equations – which are the normal forms of a 2:1 internal resonance between the two interacting modes – for $D_1 A_r$ and $D_1 A_s$, substituting the results into Equations (26) and (27) and determining the particular solutions of the latter, the ε^2-order solutions are given by [23]

$$\begin{aligned} f_{m2} = {} & \left(\frac{\Lambda_{rrs} + \Lambda_{rsr}}{4\omega_r^2}\right) A_s \bar{A}_r e^{\mathrm{i}(\omega_s - \omega_r)T_0}\delta_{mr} \\ & + \left(\frac{\Lambda_{srr}}{4\omega_s^2}\right) A_r^2 e^{2\mathrm{i}\omega_r T_0}\delta_{ms} \\ & + \left(\frac{\Lambda_{mrs} + \Lambda_{msr}}{\omega_m^2 - (\omega_s - \omega_r)^2}\right) A_s \bar{A}_r e^{\mathrm{i}(\omega_s - \omega_r)T_0}(1 - \delta_{mr}) \\ & + \left(\frac{\Lambda_{mrr}}{\omega_m^2 - 4\omega_r^2}\right) A_r^2 e^{2\mathrm{i}\omega_r T_0}(1 - \delta_{ms}) \\ & + \left(\frac{\Lambda_{mrr}}{\omega_m^2}\right) A_r \bar{A}_r + \left(\frac{\Lambda_{mss}}{\omega_m^2 - 4\omega_s^2}\right) A_s^2 e^{2\mathrm{i}\omega_s T_0} \\ & + \left(\frac{\Lambda_{mss}}{\omega_m^2}\right) A_s \bar{A}_s \\ & + \left(\frac{\Lambda_{mrs} + \Lambda_{msr}}{\omega_m^2 - (\omega_r + \omega_s)^2}\right) A_r A_s e^{\mathrm{i}(\omega_r + \omega_s)T_0} + cc, \end{aligned} \tag{29}$$

$$\begin{aligned} p_{m2} = {} & -\mathrm{i}\left(\frac{\Lambda_{rrs} + \Lambda_{rsr}}{4\omega_r}\right) A_s \bar{A}_r e^{\mathrm{i}(\omega_s - \omega_r)T_0}\delta_{mr} \\ & - \mathrm{i}\left(\frac{\Lambda_{srr}}{4\omega_s}\right) A_r^2 e^{2\mathrm{i}\omega_r T_0}\delta_{ms} \\ & + \mathrm{i}(\omega_s - \omega_r)\left(\frac{\Lambda_{mrs} + \Lambda_{msr}}{\omega_m^2 - (\omega_s - \omega_r)^2}\right) \\ & A_s \bar{A}_r e^{\mathrm{i}(\omega_s - \omega_r)T_0}(1 - \delta_{mr}) \\ & + 2\mathrm{i}\omega_r \left(\frac{\Lambda_{mrr}}{\omega_m^2 - 4\omega_r^2}\right) A_r^2 e^{2\mathrm{i}\omega_r T_0}(1 - \delta_{ms}) \\ & + 2\mathrm{i}\omega_s \left(\frac{\Lambda_{mss}}{\omega_m^2 - 4\omega_s^2}\right) A_s^2 e^{2\mathrm{i}\omega_s T_0} \\ & + \mathrm{i}(\omega_r + \omega_s)\left(\frac{\Lambda_{mrs} + \Lambda_{msr}}{\omega_m^2 - (\omega_r + \omega_s)^2}\right) \\ & A_r A_s e^{\mathrm{i}(\omega_r + \omega_s)T_0} + cc. \end{aligned} \tag{30}$$

Substituting Equations (25), (29), and (30) into the ε^3-order problem, Equation (24), imposing the solvability conditions, and using the reconstitution method, $\dot{A}_m = \varepsilon D_1 A_m + \varepsilon^2 D_2 A_m + \cdots, m = r, s$, the complex-valued modulation equations when $m = r$ and s are expressed, respectively, as

$$2\mathrm{i}\omega_r \dot{A}_r = \Re_r A_s \bar{A}_r e^{\mathrm{i}\sigma t} + K_{rr} A_r^2 \bar{A}_r + K_{rs} A_r A_s \bar{A}_s, \tag{31}$$

$$2\mathrm{i}\omega_s \dot{A}_s = \Re_s A_r^2 e^{-\mathrm{i}\sigma t} + K_{ss} A_s^2 \bar{A}_s + K_{sr} A_s A_r \bar{A}_r, \tag{32}$$

where the first-order interaction coefficients $\Re_r = \Lambda_{rrs} + \Lambda_{rsr}$ and $\Re_s = \Lambda_{srr}$. Because of the state-space form of the PDEs of motion, the Euler–Lagrange formula of system kinetic and elastic potential energies, preserving the conservative character through

Equations (31) and (32) [23], entails $\Re = \Re_r = 2\Re_s$, which governs the actual activation (non-activation) of 2:1 internal resonance when it is different from (equal to) zero [3]. Besides, it provides the intrinsic symmetry $K_{rs} = K_{sr}$. In turn, the second-order interaction coefficients governing the infinite-dimensional modal series read:

$$K_{rr} = \left\{ \overbrace{\frac{10}{3\omega_r^2}\Lambda_{rrr}^2 + \frac{9}{4\omega_s^2}\Lambda_{srr}\left(\Lambda_{rrs}+\Lambda_{rsr}\right) + 3\Gamma_{rrrr}}^{\text{resonant modes}} \right\} + \overbrace{\sum_{\substack{m=1,\\ m\neq r\neq s}}^{\infty}\left[\Lambda_{mrr}\left(\Lambda_{rrm}+\Lambda_{rmr}\right)\left(\frac{2}{\omega_m^2}+\frac{1}{\omega_m^2-4\omega_r^2}\right)\right]}^{\text{nonresonant modes}}, \tag{33}$$

$$K_{ss} = \left\{ \overbrace{\frac{10}{3\omega_s^2}\Lambda_{sss}^2 + \frac{29}{15\omega_r^2}\Lambda_{rss}\left(\Lambda_{ssr}+\Lambda_{srs}\right) + 3\Gamma_{ssss}}^{\text{resonant modes}} \right\} + \overbrace{\sum_{\substack{m=1,\\ m\neq r\neq s}}^{\infty}\left[\Lambda_{mss}\left(\Lambda_{ssm}+\Lambda_{sms}\right)\left(\frac{2}{\omega_m^2}+\frac{1}{\omega_m^2-4\omega_s^2}\right)\right]}^{\text{nonresonant modes}}, \tag{34}$$

$$K_{rs} = \overbrace{\left\{ \begin{array}{l} \frac{4\Lambda_{rss}}{15\omega_r^2}\left(\Lambda_{srs}+\Lambda_{ssr}\right) + \frac{\Lambda_{sss}}{2\omega_r^2}\left(\Lambda_{rrs}+\Lambda_{rsr}\right) + \frac{\left(\Lambda_{rrs}+\Lambda_{rsr}\right)^2}{8\omega_r^2} + \\ \frac{4\Lambda_{rss}\Lambda_{rrr}}{\omega_r^2} + 2\left(\Gamma_{rssr}+\Gamma_{rsrs}+\Gamma_{rrss}\right) \end{array} \right\}}^{\text{resonant modes}} + \overbrace{\sum_{\substack{m=1,\\ m\neq r\neq s}}^{\infty}\left[\left(\Lambda_{rms}+\Lambda_{rsm}\right)\left(\Lambda_{mrs}+\Lambda_{msr}\right)\left(\frac{1}{\omega_m^2-9\omega_r^2}+\frac{1}{\omega_m^2-\omega_r^2}\right)+\frac{2\Lambda_{mss}}{\omega_m^2}\left(\Lambda_{rrm}+\Lambda_{rmr}\right)\right]}^{\text{nonresonant modes}}, \tag{35}$$

where $K_{rs} = K_{sr}$. Evidently, each of these equations consists of two major parts, highlighting the dependence of cable response on different modal participating capacity. The first part accounts for solely the two resonant modes, consisting of both the quadratic and cubic nonlinear effects and characterizing the minimal reduced-order model. The second part, associated with quadratic nonlinearities only, corresponds substantially to the contributions from all of the nonresonant modes. The two parts are distinguished with the aim of investigating the convergence of second-order solutions, namely whether one may sufficiently account for only the two resonant (i.e., modeled) modes, or one has to consider also nonresonant (i.e., non-modeled) modes. Accordingly, in Part II [25], the first part will be kept constant for a given cable, whereas the second part will be varied according to the finite number of non-resonant modes retained up to achieving convergence.

4.2 Steady-state resonantly coupled motions

Inserting the polar form $A_m(t) = (1/2)a_m(t)e^{\mathrm{i}\beta_m(t)}$, where $m = r$ and s, into Equations (31) and (32), and then separating real and imaginary parts, the real-valued modulation equations are

$$\dot{a}_r = \frac{\Re}{4\omega_r}a_r a_s \sin\gamma, \tag{36}$$

$$a_r\dot{\beta}_r = -\frac{\Re}{4\omega_r}a_r a_s\cos\gamma - \frac{K_{rr}}{8\omega_r}a_r^3 - \frac{K_{rs}}{8\omega_r}a_r a_s^2, \tag{37}$$

$$\dot{a}_s = -\frac{\Re}{8\omega_s}a_r^2\sin\gamma, \tag{38}$$

$$a_s\dot{\beta}_s = -\frac{\Re}{8\omega_s}a_r^2\cos\gamma - \frac{K_{ss}}{8\omega_s}a_s^3 - \frac{K_{rs}}{8\omega_s}a_s a_r^2, \tag{39}$$

and describe the slow variation of amplitudes (a_r, a_s) and phases (β_r, β_s). The relative phase is given by $\gamma = \sigma t - 2\beta_r + \beta_s$. By accounting for the non-trivial contributions from the two resonant modes in Equations (37) and (39), the evolution of γ reads

$$\dot{\gamma} = \sigma + \frac{1}{16\omega_r}\left(\Re\cos\gamma\left(8-\frac{a_r^2}{a_s^2}\right)a_s + \left(4K_{rs}-K_{ss}\right)a_s^2 + \left(4K_{rr}-K_{rs}\right)a_r^2\right). \tag{40}$$

Because the periodic motion of the original system is of primary interest, the fixed points are determined

by setting $\dot{a}_r = \dot{a}_s = \dot{\gamma} = 0$. As a result, $\gamma = n\pi$, $n = 0, \pm1, \pm2, \ldots$. On accounting for second-order effects, the relationship between the amplitudes a_r and a_s reads

$$a_r = \pm\left(\frac{16a_s\omega_r\sigma + 8a_s^2\left(\Re\cos\gamma\right) + \left(4K_{rs} - K_{ss}\right)a_s^3}{\Re\cos\gamma - \left(4K_{rr} - K_{rs}\right)a_s}\right)^{\frac{1}{2}}, \tag{41}$$

in which $\Re$, K_{rr}, K_{ss}, and K_{rs} are known, whereas γ and σ are specified, for a resonant cable. For a given value of a_s, there are two real positive and negative solutions for a_r only when the argument in the bracket is positive. Thus, depending on the system parameters and quadratic/cubic coefficients, Equation (41) may have real solutions only in a certain amplitude range. The stability of the resonant nonlinear modes is evaluated by calculating the eigenvalues of the Jacobian matrix of the right-hand side of Equations (36), (38), and (40) at the fixed point. For any value of σ, the condition of marginal stability is

$$\begin{aligned}&\Re^2\left(16a_s^2 + a_r^2\right)\\ &\quad +2\Re\cos\gamma a_s^3\left(8K_{rs} - 16K_{rr} - K_{ss}\right) > 0.\end{aligned} \tag{42}$$

When keeping in Equation (42) only the first nonlinear order terms, it is found that the coupled modes are always stable [23], whereas this has to be assessed when accounting for also the second-order effects. Subsequently, based on Equations (15), (21) with $k = 2$, (25a) and (29), the polar form for A_m, the relationship $\omega_s = 2\omega_r + \varepsilon\sigma$ and the solutions of β_r and β_s from Equations (37) and (39), the second-order coupled longitudinal and vertical ($J = 1$ and 2) dynamic displacements of an internally resonant horizontal/inclined cable are expressed as

$$\begin{aligned}U^J(x,t) &\approx a_r\cos\left(\omega_r^{(N)}t + \beta_{r0}\right)\zeta_r^J(x)\\ &+ a_s\cos\left(2\omega_r^{(N)}t + 2\beta_{r0} + \gamma\right)\zeta_s^J(x)\\ &+\frac{1}{2}\begin{Bmatrix}a_s^2\left[\cos\left(4\omega_r^{(N)}t + 4\beta_{r0} + 2\gamma\right)\psi_{ss}^J(x) + \kappa_{ss}^J(x)\right]\\ +a_r^2\left[\cos\left(2\omega_r^{(N)}t + 2\beta_{r0}\right)\psi_{rr}^J(x) + \kappa_{rr}^J(x)\right]\\ +a_sa_r\left[\cos\left(3\omega_r^{(N)}t + 3\beta_{r0} + \gamma\right)\psi_{rs}^J(x)\right.\\ \left.+\cos\left(\omega_r^{(N)}t + \beta_{r0} + \gamma\right)\kappa_{rs}^J(x)\right]\end{Bmatrix},\end{aligned} \tag{43}$$

whereas the corresponding velocity fields, based on Equations (25b) and (30), are given by

$$\begin{aligned}V^J(x,t) &\approx -a_r\omega_r\sin\left(\omega_r^{(N)}t + \beta_{r0}\right)\zeta_r^J(x)\\ &-a_s\omega_s\sin\left(2\omega_r^{(N)}t + 2\beta_{r0} + \gamma\right)\zeta_s^J(x)\\ &+\frac{1}{2}\begin{Bmatrix}a_s^2\left[\sin\left(4\omega_r^{(N)}t + 4\beta_{r0} + 2\gamma\right)\hat{\psi}_{ss}^J(x)\right]\\ +a_r^2\left[\sin\left(2\omega_r^{(N)}t + 2\beta_{r0}\right)\hat{\psi}_{rr}^J(x)\right]\\ +a_sa_r\left[\sin\left(3\omega_r^{(N)}t + 3\beta_{r0} + \gamma\right)\hat{\psi}_{rs}^J(x)\right.\\ \left.+\sin\left(\omega_r^{(N)}t + \beta_{r0} + \gamma\right)\hat{\kappa}_{rs}^J(x)\right]\end{Bmatrix}\end{aligned} \tag{44}$$

The parameter ε was reabsorbed in the amplitude expressions, β_{r0} is a constant depending on the initial conditions, and κ_{ss}^J and κ_{rr}^J, which appear only in Equation (43), are static drift effects due to quadratic nonlinearities. The second-order shape functions of displacement ($\psi_{ij}^J, \kappa_{ij}^J$) and velocity ($\hat{\psi}_{ij}^J, \hat{\kappa}_{ij}^J$) are given in Appendix B, showing how the longitudinal/vertical displacements (velocities) are spatially influenced by the quadratic contributions from all of the eigenmodes. Likewise in Equations (33)–(35), the higher-order nonresonant modal contributions become progressively less significant because, in the denominators of Equations (51)–(52), either the associated frequencies appear squared or their differences with respect to the resonant frequencies in square do appear. Equations (43) and (44) are written in terms of the nonlinear frequency of the low-frequency r mode, which is given by

$$\omega_r^{(N)} = \omega_r - \left\{\left(\frac{\Re}{4\omega_r}a_s\cos\gamma\right) + \frac{K_{rr}}{8\omega_r}a_r^2 + \frac{K_{rs}}{8\omega_r}a_s^2\right\}. \tag{45}$$

It is seen that the cable response may exhibit softening or hardening nonlinearity, depending on the specified γ and the contributions from first- and second-order nonlinear coefficients multiplying the amplitudes (a_r,a_s) in the bracket. On the other hand, when expressing the nonlinear frequency in terms of the high-frequency s mode, it can be proved that the nonlinear resonance tunes the phases of the resonant modes so that $\omega_s^{(N)} = 2\omega_r^{(N)}$ (see, e.g. [36]). Equations (43) and (44) show the $a_r - a_s$ amplitudes dependence of the dynamic configuration and velocity fields, and their second-order spatial corrections, whereas Equation (45) highlights

the $a_r - a_s$ amplitudes dependence of the nonlinear frequencies and their second-order corrections.

4.3 Some remarks

4.3.1 Multiple internal resonances

Depending on cable parameters, Equations (33)–(35) reveal how the solutions may break down when other internal resonances come into play, corresponding to the involvement of other non-modeled, usually higher-frequency m planar modes, and a multiple resonance activation. Indeed, the latter occurs in horizontal cables, typically at crossovers, when considering also out-of-plane modes [8–12]. However, depending on the frequency tuning, a multiple *planar* resonance is more likely to occur in inclined cables because of the vanishing of nonlinear orthogonality of coupled modes ensuing from the incompletely symmetric or anti-symmetric spatial character of inclined configurations, as will be discussed in Part II [25]. For instance, a further 2:1 resonance may occur near second ($\omega_m \approx 2\omega_r$) or third ($\omega_m \approx 2\omega_s$) avoidance in the relevant frequency spectrum, leading to a multiple 2:2:1 or 4:2:1 resonance, respectively. A further 1:1 resonance ($\omega_m \approx \omega_r$) may occur near avoidance, involving the two coexisting hybrid modes [20] and giving rise to a multiple 2:1:1 resonance. Moreover, a further 3:1 resonance ($\omega_m \approx 3\omega_r$) may occur and entail a multiple 3:2:1 resonance. The activation of multiple *planar* resonances has numerically been observed in Srinil et al. [20] and [37] for the 4:2:1 or 3:2:1 resonance occurring in a low-extensible inclined or high-extensible horizontal cable, respectively. Yet, such conditions are beyond the scope of the present study.

4.3.2 Nonlinear coefficients

Though being not explicit, in Equations (19) or (20), the single quadratic or cubic coefficients may have either positive or negative values, depending on the relative contributions from the static equilibrium (parabolic or cubic-order) solutions, the modal eigenfunctions and their relative phases. Accordingly, for a different number of retained modes, there is a possibility of sign difference in the resulting second-order quadratic coefficients in Equations (33)–(35) or (51)–(52), depending on the outcome of each component quadratic coefficient, on their combination, and on the system frequency commensurability. In evaluating the latter, we disregard the higher-order effects of the 2:1 resonance detuning in Equations (33)–(35) and (51)–(52).

4.3.3 Dynamic displacement solutions

With M being the order of modal truncation, the second-order dynamic displacements, Equation (43), account for the second-order effects of quadratic nonlinearities in both the amplitudes, Equation (41), and frequencies, Equation (45). When truncating Equation (43) after the first-order terms, the associated solutions may be considered as first-order (improved first-order) displacements when accounting for the first-order (first- and second-order) amplitudes/frequencies [1]. Thus, it is remarked that the improved first-order displacements account for solely the shapes of resonant modes, whose time-dependence is, however, governed by the second-order frequencies/amplitudes, whereas the second-order displacements account for also the spatial corrections from all retained modes.

4.3.4 Nonplanar 2:1 resonance

The same line of MMS analysis as in the planar 2:1 resonance can be pursued to address a nonplanar 2:1 resonance involving in-plane/out-of-plane (s, r) modes by considering the complete set of Equations (17)–(18) with the relevant coefficients in (19)–(20). To this end, the structure of modulation Equations (31)–(32), the resonant amplitudes (41) and frequency-amplitudes (45) relationships, and even the stability criterion (42) are the same for planar and nonplanar interactions. Though being the first- and second-order interaction coefficients different [14], activation of a nonplanar 2:1 resonance is still governed by the condition $\Re = \Re_r = 2\Re_s \neq 0$, in which, however, $\Re_r = \Psi_{rrs}$ and $\Re_s = \vartheta_{srr}$ for the nonplanar interaction.

5 Approximate model validation

Prior to parametrically studying the nonlinear dynamics of the approximate model through the MMS solution in Part II [25], the analytical solutions obtained for cable statics and linear dynamics, as well as the nonlinear dynamic solutions of the approximate PDEs, are validated through various numerical solutions of the exact model. To gain insight into the significance of

system longitudinal dynamics and their effects on the nonlinear response, the 2:1 resonant interaction coefficients of the approximate non-condensed/condensed horizontal cable models are also examined. A low-extensible cable with a fixed non-dimensional parameter $EA/w_C X_H \approx 2580.35$ is analyzed, which has $X_H = 850\,\text{m}$, $A = 0.1159\,\text{m}^2$, $w_C \approx 9.48\,\text{kN/m}$ and $E = 1.794 \times 10^8\,\text{kN/m}^2$ [20]. Reference is also made to the parameter λ/π that governs the horizontal/inclined cable dynamics and the corresponding crossover/avoidance phenomena, see Part II [25].

5.1 Horizontal/inclined static configurations

The equation governing the static configuration of the exact model is the same as Equation (10), when multiplying the denominator in its right-hand side by $(1 + e)$ [21]. To obtain numerical solutions of arbitrarily sagged and inclined cables, both the hybrid fourth-order Runge-Kutta/Shooting method (RKS) and the finite element method (FEM, 50 elements) with a cubic polynomial function in x are considered, for a specified end tension problem [14]. In each considered case, the associated tension H is evaluated and used in Equation (11) to obtain the closed-form Irvine's solution (IRV) for the vertical configuration. Results of small and quite large values of the sag-to-span ratio d for horizontal (HC1 and HC2) and inclined ($\theta = 60^\circ$, IC1 and IC2) cables, and the associated parameters α, are comparatively reported in Table 1a and b, the latter also reporting the parameter $\varepsilon*$ of inclined cables. The corresponding configurations are displayed in Figs. 2 and 3.

The numerical and analytical results in Table 1 are in good agreement for the shallow ($d < 1{:}8$) horizontal cable (HC1, Fig. 2a) and even for the intermediate-sagged ($d > 1{:}8$, $\varepsilon* < 1$) inclined cable (IC1, Fig. 3a). For larger-sagged cables, the RKS and FEM results remain in excellent agreement, but they differ from the IRV ones owing to the invalidity of the latter in describing the large-sagged cable ($d \gg 1{:}8$, $\varepsilon* > 1$). The IRV solution predicts underestimated (overestimated) d values for HC2 (IC2). However, its deviation from numerical solutions is clearly seen in Fig. 2b for HC2, as expected due to the completely invalid parabolic approximation, whereas a smaller difference occurs regarding the inclined configurations in Fig. 3b. Depending on the cable parameter, Fig. 3b highlights that, even if the inclination angle is high ($\theta = 60^\circ$) and the associated d ($\varepsilon*$) value is large, the results given by Equation (11) accounting for also the asymmetry effects remain satisfactorily valid when compared with RKS and FEM results. This allows the parametric studies in [25] to include not only small-sagged horizontal/inclined cables but also possibly moderately large-sagged inclined cables.

Table 1 Comparison of d with numerical and analytical solutions: (a) horizontal cables, (b) inclined cables

			d		
Cable	α	$\varepsilon*$	RKS	FEM	IRV
(a)					
HC1	2286.6		0.112	0.112	0.111
HC2	4482.1		0.231	0.231	0.217
(b)					
IC1	2286.9	0.768	0.220	0.220	0.222
IC2	4431.5	1.487	0.423	0.423	0.436

5.2 Linear planar/nonplanar dynamics

The equations of motion governing the cable linear vibration of the exact and approximate models are the same [14], apart from the term $(1 + e)$ also appearing in the former, see Equations (2)–(4). The natural frequencies and mode shapes of the approximate model obtained by the Galerkin method with a sine-based series (GMS) are validated by the FEM results of the exact model. By properly varying the number N of retained terms in the series, the convergence of the GMS solution must be first fulfilled. Then, with a guaranteed N, the agreement between GMS and FEM out-of-plane/in-plane frequencies must be achieved for various small-sagged horizontal and inclined cables in the first three crossover/avoidance regions [14].

Here, a comparison of the normalized first two out-of-plane (O1–O2) and first four in-plane (I1–I4) mode shapes (τ) of the two solutions is exemplified in Fig. 4 for the second avoidance ($\lambda/\pi \approx 4$) inclined cable ($\alpha \approx 1436.9$) with $\theta = 45^\circ$. Apart from justifying both the parabolic static profile and $\rho \approx 1$ assumptions in the linear dynamics of the approximate horizontal cables [14], the excellent agreement between GMS and FEM mode shapes of the inclined cable is highlighted. Essentially, the properly truncated sine-based

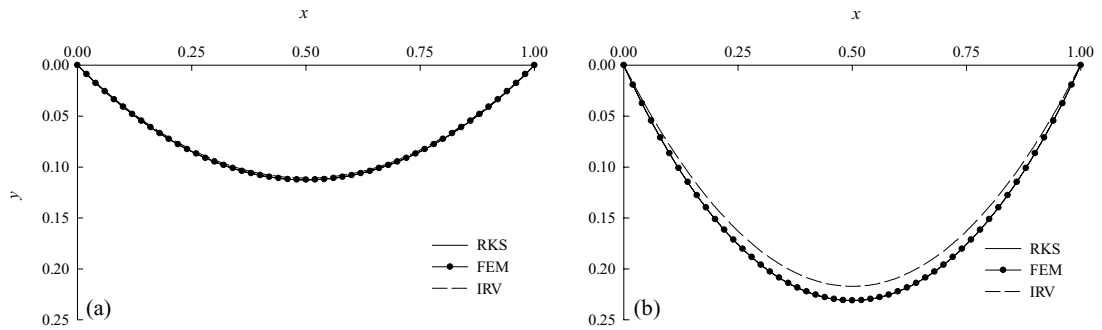

Fig. 2 Comparison of horizontal static configurations with numerical and analytical solutions: (a) $\alpha \approx 2286.6$; (b) $\alpha \approx 4482.1$

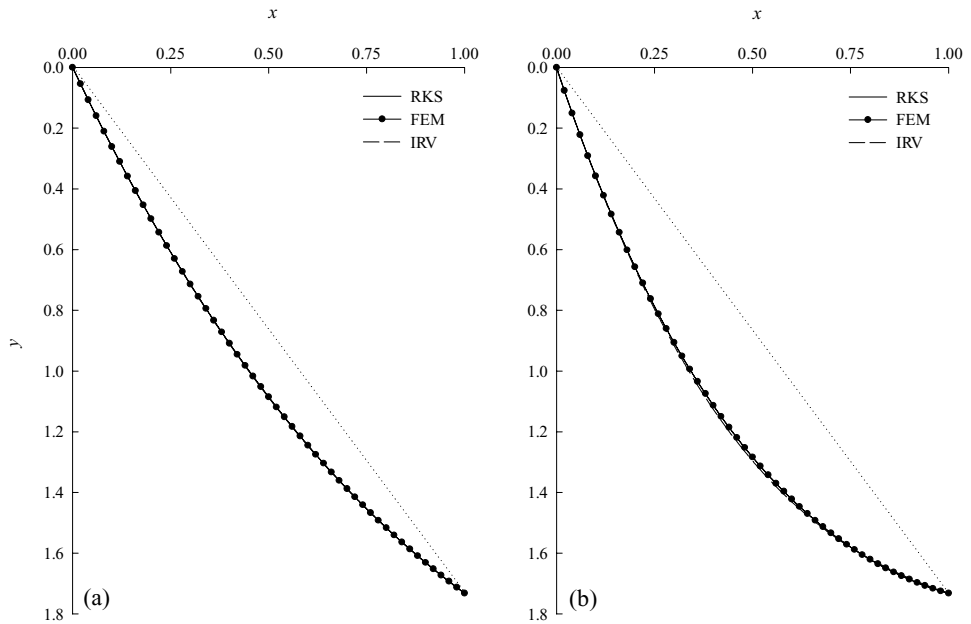

Fig. 3 Comparison of inclined ($\theta = 60^\circ$) static configurations with numerical and analytical solutions: (a) $\alpha \approx 2286.9$; (b) $\alpha \approx 4431.5$

series ($N = 15$) is seen capable of describing – besides the symmetric/anti-symmetric nonplanar w (O1/O2) modes, and the *nearly* anti-symmetric (I1) and symmetric (I2) u/v planar modes – also the *hybrid* u/v planar modes coexisting at second avoidance (I3, I4).

5.3 Nonlinear planar/nonplanar dynamics

Numerical time histories of the exact, (2)–(4), and approximate, (7)–(9), PDEs of cable motion are now analyzed and compared by the finite difference method with central approximation of both spatial (50 elements) and temporal (time step = 0.0001 s) derivatives [14]. The differentiated PDEs of the approximate model are given, in dimensional form, in Appendix C, whereas those of the exact model have been reported in [21]. It is worth remarking that, for the approximate horizontal cable, two cases are considered for a better model selection, namely (i) $\rho \approx 1$ which is consistent with the parabolic assumption employed in both statics and linear dynamics, and (ii) the spatially varying ρ terms as they actually appear in Equations (7)–(9). Accordingly, the terms divided by ρ^6 are absent in Equations (53)–(55) for the (i) case, whereas the full system equations hold for the (ii) case and for inclined cables. In the following, nonplanar (planar) nonlinear free responses initiated by a single-mode out-of-plane (in-plane) spatial displacement with prescribed vibration amplitude (a_p) and zero velocity are displayed for some resonant horizontal/inclined cables.

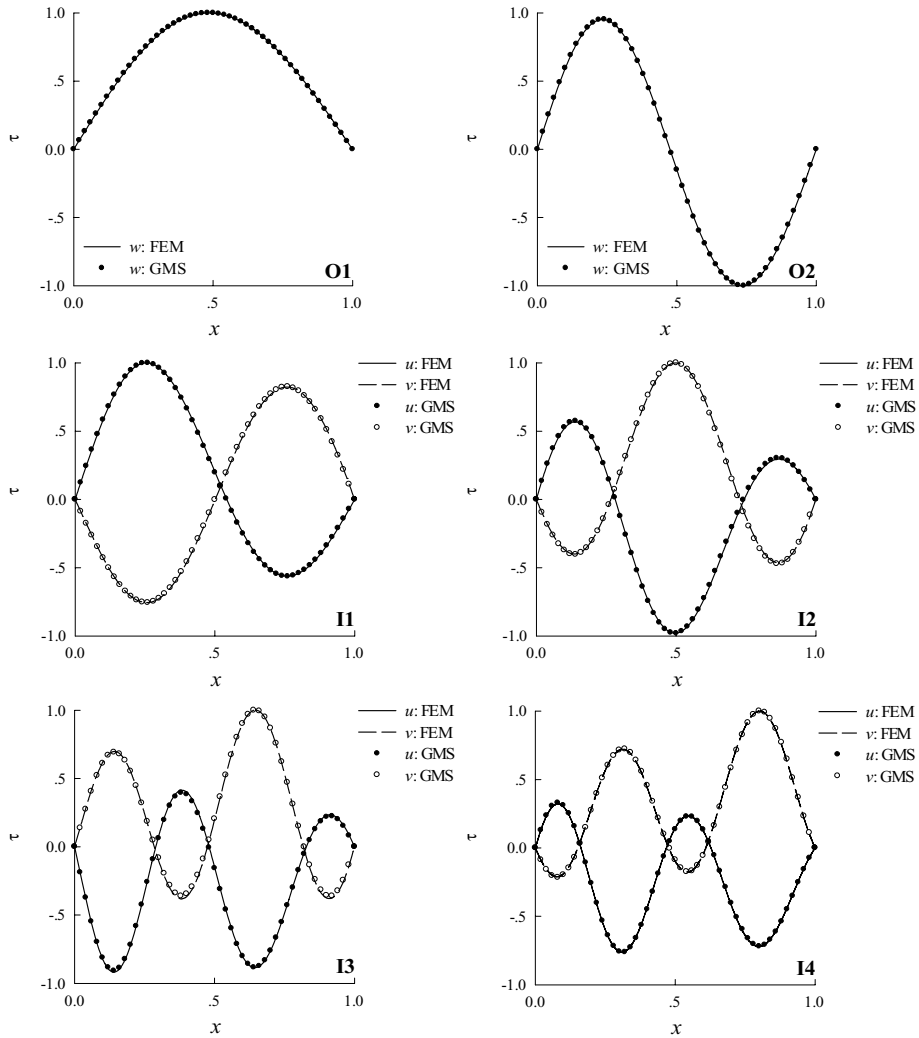

Fig. 4 Comparison of two out-of-plane (O1, O2) and four in-plane (I1–I4) FEM and GMS modes for second-avoidance inclined ($\theta = 45^\circ$) cable with $\alpha \approx 1436.9$

The v and w responses at mid-span, initiated by the first symmetric out-of-plane mode with $a_p = 2.5\,\mathrm{m}$, are shown in Fig. 5, for the first-crossover horizontal cable ($\alpha \approx 639.4$). The responses of the exact model (solid lines) and of the approximate model with varying ρ-terms (circles) are seen to be in close agreement, whereas those of the approximate model with $\rho \approx 1$ (dotted lines) exhibit meaningful differences. Such discrepancies are more evident in the planar (v) than in the nonplanar (w) responses because the neglected ρ-terms are associated with planar statics, and occur even though overall qualitative agreement is found, i.e., a beating-type phenomenon due to activation of the nonplanar 2:1 resonance involving the driven (v) and exciting (w) first-symmetric modes [21]. Thus, accounting for the varying ρ-terms in the approximate *nonplanar* model of *horizontal* cables looks preferable.

When considering the second-avoidance inclined ($\theta = 60^\circ$) cable ($\alpha \approx 2016.5$) initiated by the first anti-symmetric out-of-plane mode with $a_p = 2.5\,\mathrm{m}$, a small difference occurs between the results obtained with the exact and approximate (varying ρ-terms) models, as shown in Fig. 6, which plots the relevant u, v, and w responses at quarter span from left support. Again, all nonlinear responses highlight a modal interaction due to the nonplanar 2:1 resonance involving the driven high-frequency (third

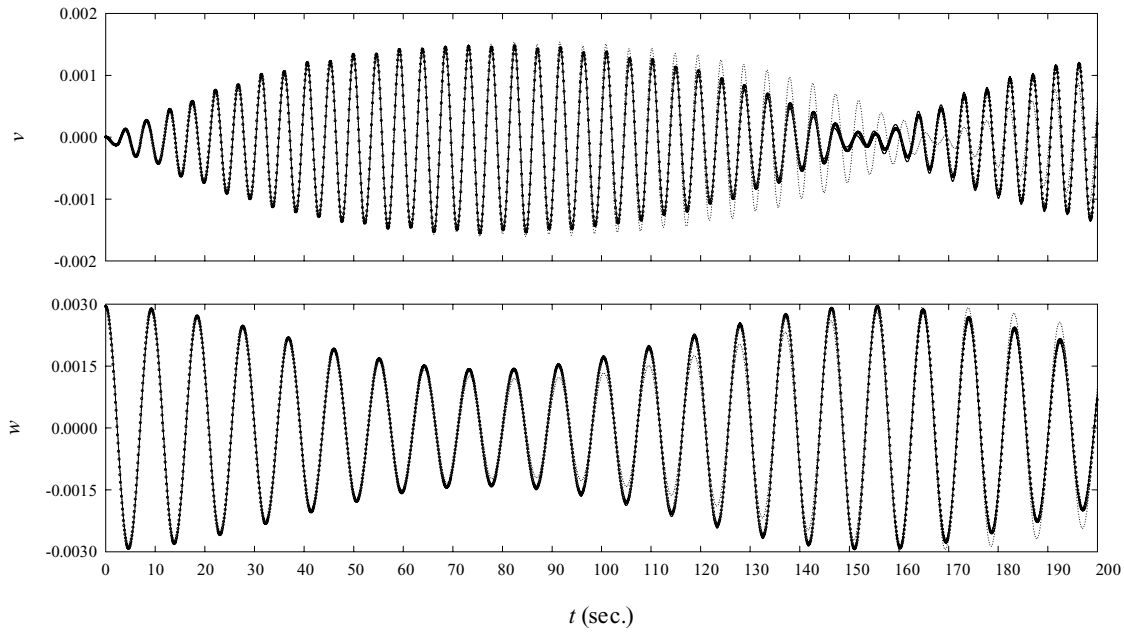

Fig. 5 Comparison of v and w nonlinear responses initiated by first symmetric out-of-plane mode for first-crossover horizontal cable with $\alpha \approx 639.4$: solid lines (dotted lines or circles) denote exact model (approximate model with $\rho \approx 1$ or varying ρ-terms)

or fourth) planar mode and the initiated nonplanar mode [20]. Therefore, the results also justify using the approximate *nonplanar* model for *inclined* cables.

As regards *planar* vibrations, a remarkable quantitative difference in the responses obtained with the three models occurs for the considered non-crossover horizontal cable with $\lambda/\pi \approx 2.95$, as visualized in Fig. 7, which plots the u/v responses at 1/8 span initiated by the second in-plane mode with $a_p = 1$ m. It can be seen that, with respect to the exact model responses, those of the approximate model with $\rho \approx 1$ exhibit greater errors (see also the more hardening nonlinearity) than those of the approximate model with varying ρ-terms, as clearly shown by the enlarged view of v response in the resonant interaction t-range. This occurs because of the definitely major influence of the ρ-terms in the purely planar dynamics. Thus, depending on also the vibration amplitudes, there are clear hints about the need to consider the actual varying ρ-terms in the approximate *planar* model of *horizontal* cables and in the subsequent MMS-based parametric study [25], contrary to what is currently done in the relevant literature [1]. With the same λ/π and a_p values, the difference between approximate and exact model responses decreases for the inclined cable with $\theta = 45^\circ$ shown in Fig. 8. This thoroughly validates using the approximate *planar* model also for *inclined* cables.

Overall, the amplitude-modulated features of all models in Figs. 7 and 8 exhibit qualitative agreement, as confirmed by the associated Fourier amplitude densities in Fig. 9 (v) and 10 (u), respectively. In particular, they substantially highlight two major frequencies corresponding to the fifth and second planar modes, the formers being periodically dragged in the response due to their involvement in the nearly tuned 2:1 resonance for the $\lambda/\pi \approx 2.95$ horizontal (non-crossover) or inclined (non-avoidance) cable (see [25]). The approximate horizontal cable model with $\rho \approx 1$ still exhibits a major discrepancy versus the others as regards the amplitudes of the two resonant peaks in Fig. 9.

5.4 Longitudinal displacement contributions and kinematic condensation effects

Depending on the cable sag and/or extensibility, the contributions of longitudinal displacement are now examined in a horizontal cable through the 2:1 resonant coefficients of the MMS solution. Attention is first focused on the *cubic* coefficients which, based on the outcomes in Section 5.3, are evaluated for the non-crossover ($\lambda/\pi \approx 2.95$, $r = 2$, $s = 5$, $N = 20$) and second-crossover ($\lambda/\pi \approx 4.03$, $r = 1$, $s = 4$, $N = 40$) cables – both having low extensibility ($E = O(10^8)$ or $E = O(10^7)$) – by using the

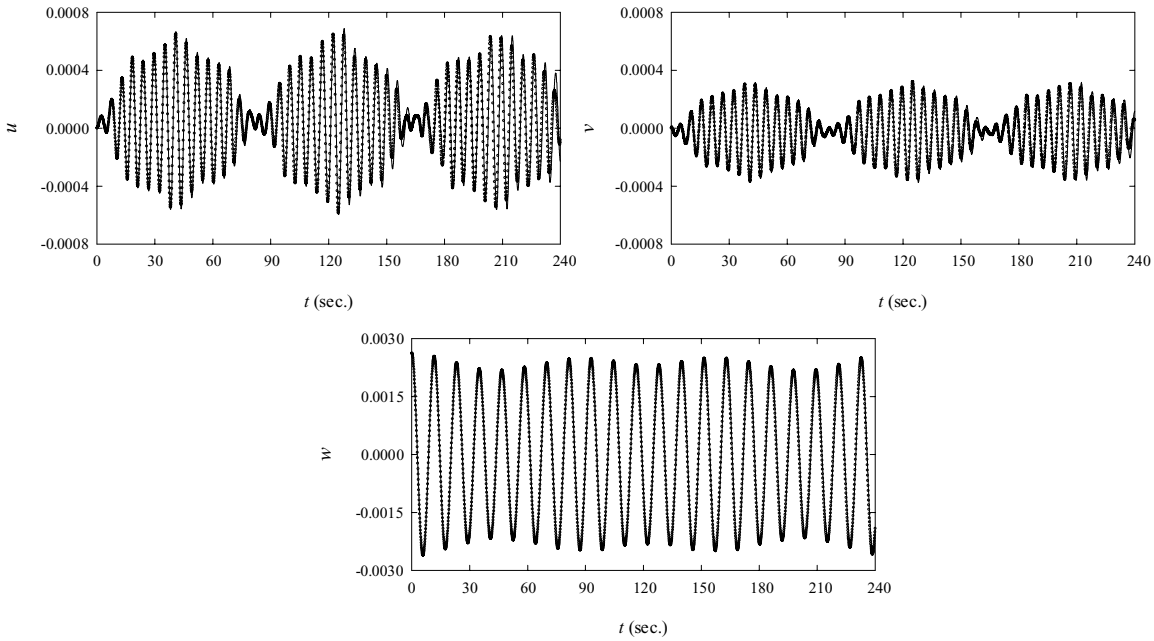

Fig. 6 Comparison of u, v, and w nonlinear responses initiated by first anti-symmetric out-of-plane mode for second-avoidance inclined ($\theta = 60^\circ$) cable with $\alpha \approx 2016.5$: solid lines (circles) denote exact (approximate) model

Table 2 Percent contributions to cubic coefficients governing 2:1 internal resonance due to longitudinal/vertical displacements of different sagged (λ/π) and extensible (E) cables

			$E = O(10^8)$		$E = O(10^7)$	
λ/π	K	Γ	U-V (%)	V (%)	U-V (%)	V (%)
2.95	K_{rr}	Γ_{rrrr}	0.651	99.349	2.489	97.511
	K_{ss}	Γ_{ssss}	1.742	98.258	7.046	92.954
	K_{rs}	Γ_{rssr}	1.362	98.638	5.373	94.627
		Γ_{rsrs}	1.278	98.722	4.923	95.077
		Γ_{rrss}	1.290	98.710	4.916	95.084
4.03	K_{rr}	Γ_{rrrr}	3.025	96.975	11.845	88.155
	K_{ss}	Γ_{ssss}	2.014	97.986	9.138	90.862
	K_{rs}	Γ_{rssr}	2.101	97.899	9.595	90.405
		Γ_{rsrs}	2.141	97.859	9.709	90.291
		Γ_{rrss}	2.379	97.621	10.737	89.263

approximate non-condensed model which accounts for the ρ-term effects. Remark also that the cable with $\lambda/\pi \approx 2.95$ (4.03) involves anti-symmetric/anti-symmetric (symmetric/anti-symmetric) *longitudinal* resonant r/s components. As given by Equation (19d), the generic cubic coefficient Γ_{mijk}, solely depending on the two resonant modes in Equations (33)–(35), consists of four additive terms: the first three terms (labeled U-V) account for both longitudinal (ϕ) and coupled longitudinal–vertical (ϕ–φ) displacement contributions, whereas the last term (labeled V) exhibits the solely vertical φ displacement dependence. The separate percent contributions of U-V and V terms to each of the coefficients $\Gamma_{rrrr}, \Gamma_{ssss}, \Gamma_{rssr}, \Gamma_{rsrs}, \Gamma_{rrss}$, entering K_{rr}, K_{ss}, and K_{rs} (Equations (33)–(35)), are reported in Table 2.

For the smaller-sagged cable with $\lambda/\pi \approx 2.95$, contributions from U-V are seen to be very small with respect to those from V, as expected from a physical standpoint. This validates, for low-sagged (and low-extensible) cables, the common use of indirectly accounting for the longitudinal contribution to cubic coefficients, as well as to quadratic ones, through its solely condensed effect in the unique

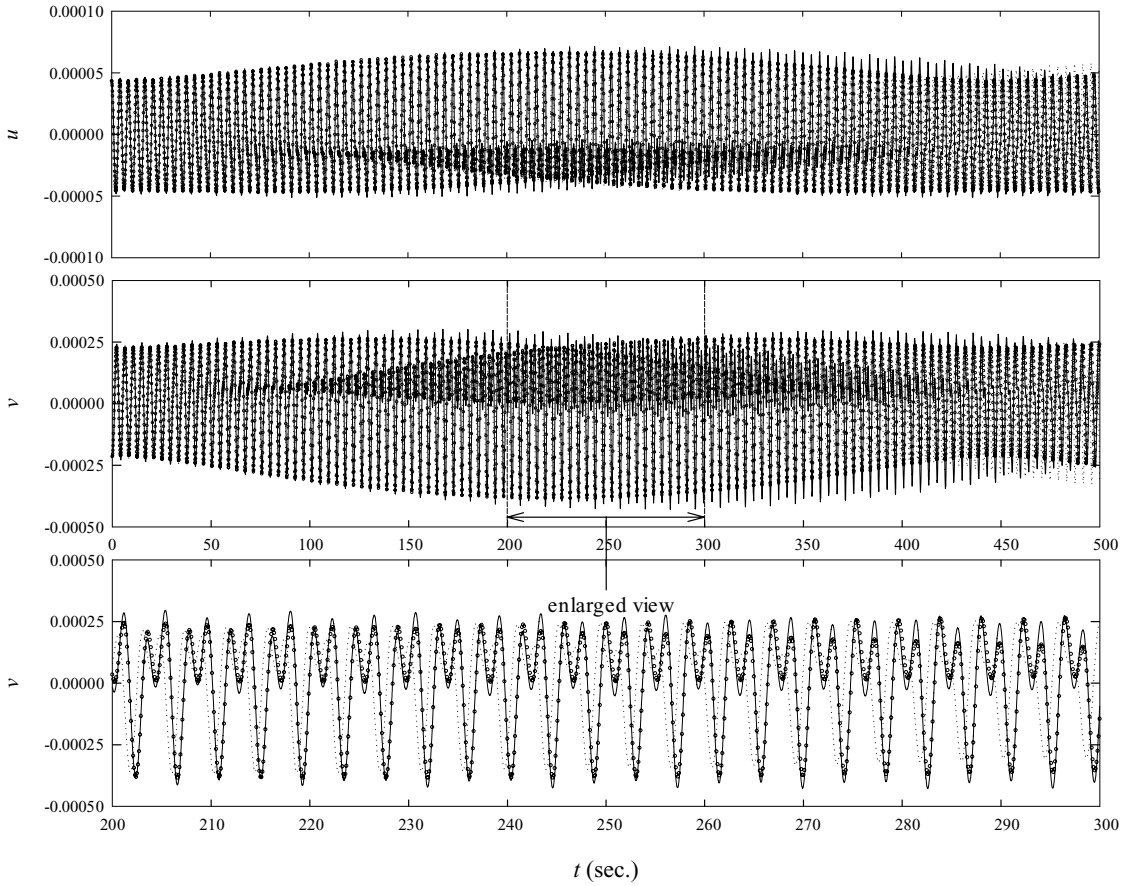

Fig. 7 Comparison of u and v nonlinear responses initiated by second in-plane mode for horizontal cable with $\lambda/\pi \approx 2.95$: solid lines (dotted lines or circles) denote exact model (approximate model with $\rho \approx 1$ or varying ρ-terms)

vertical φ displacement term in Equation (20d). However, the effect of U-V terms somehow increases as the cable sag is increased to $\lambda/\pi \approx 4.03$ (with the fixed EA parameter), and it becomes as more apparent as cable extensibility is higher (lower E), for a given λ/π. Of course, the overall discrepancy between different models has to be evaluated in the second-order interaction coefficients, which are influenced – depending on the modal (longitudinal/vertical) shape character and magnitude – by their additive cubic-based, as well as multiple quadratic-based, expressions having variable resonant/nonresonant modal participating capacity, see Equations (33)–(35).

Thus, it is worth examining and comparing the second-order quadratic/cubic coefficients obtained with the non-condensed/condensed modeling. A larger-sagged horizontal cable ($\lambda/\pi \approx 5.48$, $E = O(10^8)$) exhibiting symmetric/symmetric modal interaction ($r = 2,\ s = 5$) is considered (Table 3), by accounting for the first 15 modes. Their percent differences (P) with respect to the non-condensed ($N = 30$) coefficients are also given. The superscript 'q' ('c') denotes the quadratic (cubic) contribution to K_{ii}. Overall, the two models provide qualitative agreement as regards the sign (softening- or hardening-type nonlinearity) of quadratic and cubic coefficients. Nonetheless, there are remarkable quantitative differences in all coefficients, the percent values being outstandingly greater for the *cubic* coefficients, especially for K_{rs} ($P \approx 62.38\%$).

From a computational point of view, such meaningful differences seem to be reasonable because only the non-condensed coefficients are influenced by also the U-V terms, which are significant (Table 2) for the considered larger-sagged cable. Recall also that the non-condensed (condensed) cubic coefficients are (are not) influenced by the ρ^3-dependent terms. As regards the differences between the quadratic/cubic contributions

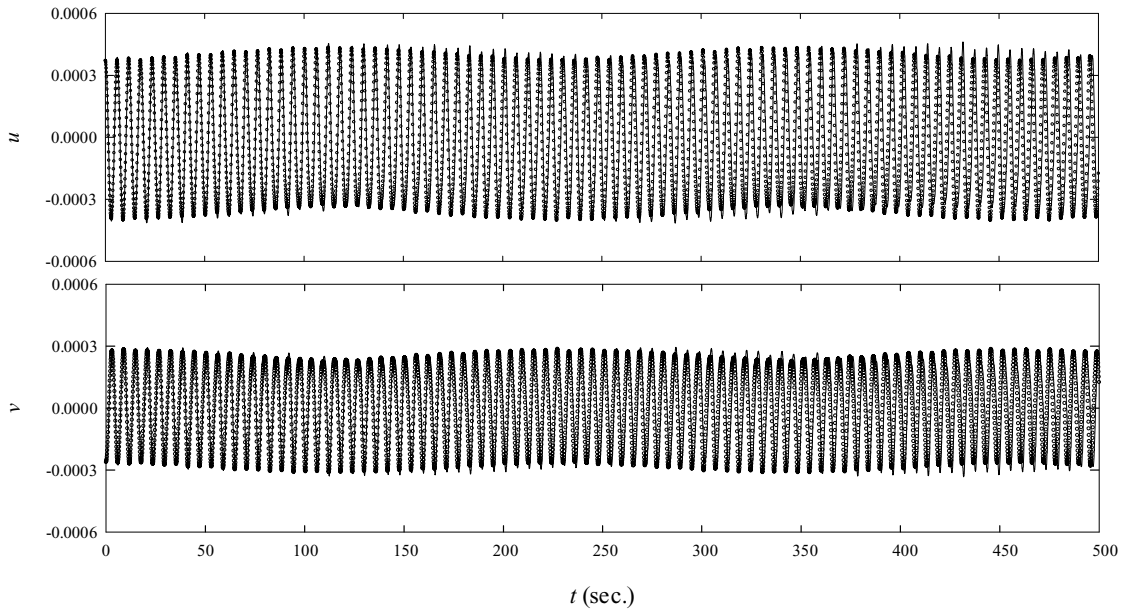

Fig. 8 Comparison of u and v nonlinear responses initiated by second in-plane mode for inclined ($\theta = 45^\circ$) cable with $\lambda/\pi \approx 2.95$: solid lines (circles) denote exact (approximate) model

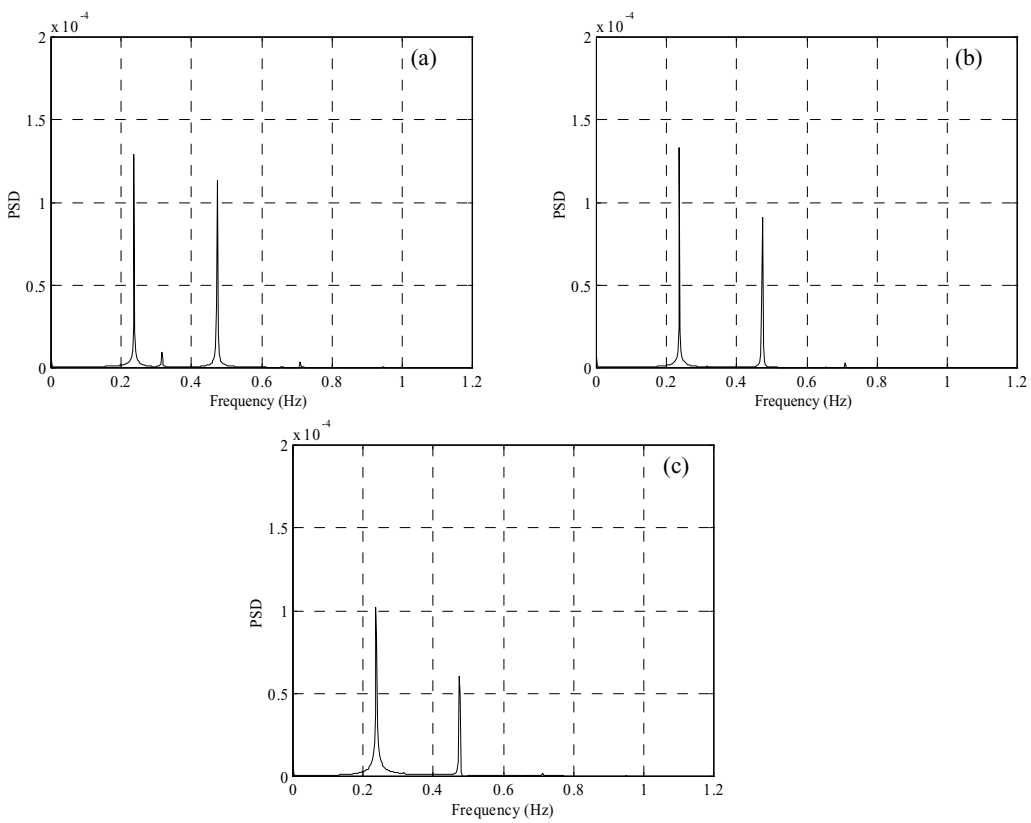

Fig. 9 Fourier amplitude densities of v responses in Fig. 7: (a) exact model, approximate model with (b) varying ρ-terms and (c) $\rho \approx 1$

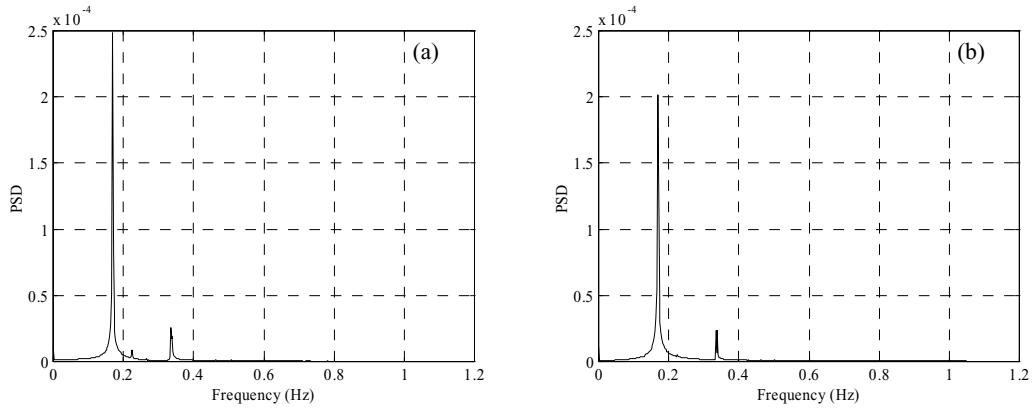

Fig. 10 Fourier amplitude densities of u responses in Fig. 8: (a) exact model, (b) approximate model

Table 3 Comparison of second-order quadratic/cubic coefficients governing 2:1 resonance with two physical models and their percent differences for horizontal cable with $\lambda/\pi \approx 5.48$

K	Non-condensed model	Condensed model	P (%)
K_{rr}^{q}	6305837.166	6783535.666	7.58
K_{rr}^{c}	−15419441.480	− 10229946.306	33.66
K_{ss}^{q}	102345334.304	111981072.099	9.41
K_{ss}^{c}	−41994120.481	−31180837.908	25.75
K_{rs}^{q}	13095299.468	13821561.521	5.55
K_{rs}^{c}	−36143334.648	−13598798.289	62.38

or the pure (K_{hh}, $h = r$ or s)/mixed (K_{rs}) coefficients, consider (i) that each term in the cubic (quadratic) coefficients ensues from a multiplication of four (three) modal shapes, see Equations (19d) (19a) and (20d) (20a), and (ii) that there are totally six additive components in the cubic component of K_{rs} ($2\Gamma_{rssr} + 2\Gamma_{rsrs} + 2\Gamma_{rrss}$) instead of three additive components in that of K_{hh} ($3\Gamma_{hhhh}$). As a result, the condensed model exhibits smaller (larger) absolute values of cubic (quadratic) coefficients. The underlying mechanical meaning is that the condensed model reduces (strengthens) the degree of hardening (softening) nonlinearities through Equation (45), since the higher-order effects of longitudinal dynamic deformation due to cable nonlinear stretching are neglected through the kinematic condensation. Consequently, there is a possibility of different contributions, simply evaluated by the summation of quadratic and cubic coefficients, to the overall response nonlinearities. In Table 3, the summation of K_{rs} provides a negative value (−23,048,035.180) for the non-condensed model against a positive value (222, 763.233) for the condensed model. Such considerable differences in the values and/or in the sign of some effective coefficients are capable of influencing the resulting coupled dynamics of the two distinctive models.

6 Concluding remarks

Based on a general *kinematically non-condensed* model valid for horizontal/inclined cables, the approximate equations of geometrically nonlinear undamped unforced 3-D coupled motion accounting for dynamic extensibility (i.e., space–time dynamic strain variation) and system asymmetry due to inclined sagged configurations have been presented. With the aim of analytically investigating the planar 2:1 resonant, multimodal, free dynamics of horizontal/inclined cables, approximate closed-form solutions for small sagged cables have been accomplished by means of a multidimensional Galerkin discretization and a second-order multiple scales approach. The analytical outcomes highlight the higher-order effects due to system quadratic nonlinearities on the resonantly coupled amplitudes, frequencies, dynamic configurations and velocities associated with the *resonant nonlinear normal modes*. The dependence of cable response on different resonant/nonresonant (modeled/non-modeled) modal contributions has been emphasized. Accuracy of approximate horizontal/inclined cable models has thoroughly been validated by numerically evaluating the associated static as well as nonplanar/planar linear and nonlinear dynamic results against those of the exact model. Overall qualitative agreement of *approximate* and *exact* model results has been found, apart from some quantitative differences, depending on the element kinematics description, system parameters and consideration of planar or nonplanar dynamics.

Finally, significant insights into the modal coupling role played by system longitudinal dynamics and the effects of disregarding their higher contributions on nonlinear coefficients through kinematic condensation have been obtained for horizontal cables, by also highlighting the influence of cable sag and/or extensibility.

The overall model verifications and the exhibited strain condensation effects entitle us to use the accomplished MMS solution of the *approximate non-condensed* horizontal/inclined cable model to ascertain the main spatio-temporal features of the nonlinear dynamics due to planar 2:1 resonances. This will be conducted in Part II [25].

Appendix A

For the condensed model of shallow horizontal cables, the integro-partial differential equations of motion describing the vertical and out-of-plane displacements read [9]

$$\ddot{v} = v''+\alpha(y''+v'')\int_0^1\left(y'v'+\frac{1}{2}(v'^2+w'^2)\right)dx, \tag{46}$$

$$\ddot{w} = w''+\alpha w''\int_0^1\left\{y'v'+\frac{1}{2}(v'^2+w'^2)\right\}dx. \tag{47}$$

where $y \approx 4dx(1-x)$. For vertical anti-symmetric (out-of-plane) modes, the frequencies are $\omega_n = n\pi, n = 2, 4, \ldots (1, 2, 3, \ldots)$, where the associated mode shapes read

$$\varphi_n(x) = \xi_n(x) = \sqrt{2}\sin(n\pi x). \tag{48}$$

For vertical symmetric modes $(n = 1, 3, \ldots)$, the frequencies are the roots of

$$\frac{1}{2}\omega_n - \tan\left(\frac{1}{2}\omega_n\right) - \frac{1}{2\lambda_C^2}(\omega_n)^3 = 0, \tag{49}$$

where $\lambda_C^2 = 64d^2\alpha$ [13], with $d \approx w_C X_H/8H$ and $\alpha = EA/H$. The relevant symmetric vertical mode shapes are given by

$$\varphi_n(x) = C_n\left[1-\tan\left(\frac{1}{2}\omega_n\right)\sin(\omega_n x)-\cos(\omega_n x)\right], \tag{50}$$

where C_n is arbitrary. Equations (48) and (50) are determined such that

$$\int_0^1 \varphi_n^2 dx = \int_0^1 \xi_n^2 dx = 1.$$

Appendix B

The pertinent second-order shape functions showing the contributions from resonant and nonresonant modes to the displacements in Equation (43) are given by

$$\psi_{rr}^J(x) = -\frac{\Lambda_{rrr}}{3\omega_r^2}\zeta_r^J(x)+\frac{\Lambda_{srr}}{4\omega_s^2}\zeta_s^J(x) + \sum_{\substack{m=1,\\ m\neq r\neq s}}^{\infty}\left(\frac{\Lambda_{mrr}}{\omega_m^2-4\omega_r^2}\zeta_m^J(x)\right), \tag{51a}$$

$$\psi_{ss}^J(x) = -\frac{\Lambda_{rss}}{15\omega_r^2}\zeta_r^J(x)-\frac{\Lambda_{sss}}{3\omega_s^2}\zeta_s^J(x) + \sum_{\substack{m=1,\\ m\neq r\neq s}}^{\infty}\left(\frac{\Lambda_{mss}}{\omega_m^2-4\omega_s^2}\zeta_m^J(x)\right), \tag{51b}$$

$$\psi_{rs}^J(x) = -\frac{\Lambda_{rrs}+\Lambda_{rsr}}{8\omega_r^2}\zeta_r^J(x)-\frac{\Lambda_{srs}+\Lambda_{ssr}}{5\omega_r^2}\zeta_s^J(x) + \sum_{\substack{m=1,\\ m\neq r\neq s}}^{\infty}\left(\frac{\Lambda_{mrs}+\Lambda_{msr}}{\omega_m^2-9\omega_r^2}\zeta_m^J(x)\right), \tag{51c}$$

$$\kappa_{rs}^J(x) = \frac{\Lambda_{rrs}+\Lambda_{rsr}}{4\omega_r^2}\zeta_r^J(x)+\frac{\Lambda_{srs}+\Lambda_{ssr}}{3\omega_r^2}\zeta_s^J(x) + \sum_{\substack{m=1,\\ m\neq r\neq s}}^{\infty}\left(\frac{\Lambda_{mrs}+\Lambda_{msr}}{\omega_m^2-\omega_r^2}\zeta_m^J(x)\right), \tag{51d}$$

$$\kappa_{rr}^J(x) = \frac{\Lambda_{rrr}}{\omega_r^2}\zeta_r^J(x)+\frac{\Lambda_{srr}}{\omega_s^2}\zeta_s^J(x)$$

$$+\sum_{\substack{m=1,\\ m\neq r\neq s}}^{\infty}\frac{\Lambda_{mrr}}{\omega_m^2}\zeta_m^J(x), \tag{51e}$$

$$\kappa_{ss}^J(x)=\frac{\Lambda_{rss}}{\omega_r^2}\zeta_r^J(x)+\frac{\Lambda_{sss}}{\omega_s^2}\zeta_s^J(x)+\sum_{\substack{m=1,\\ m\neq r\neq s}}^{\infty}\frac{\Lambda_{mss}}{\omega_m^2}\zeta_m^J(x), \tag{51f}$$

whereas those to the associated velocities in Equation (44) are given by

$$\hat{\psi}_{rr}^J(x)=\frac{2\Lambda_{rrr}}{3\omega_r}\zeta_r^J(x)+\frac{\Lambda_{srr}}{4\omega_s}\zeta_s^J(x)+\sum_{\substack{m=1,\\ m\neq r\neq s}}^{\infty}\left[\frac{-2\omega_r\Lambda_{mrr}}{\omega_m^2-4\omega_r^2}\zeta_m^J(x)\right], \tag{52a}$$

$$\hat{\psi}_{ss}^J(x)=\frac{4\Lambda_{rss}}{15\omega_r}\zeta_r^J(x)+\frac{2\Lambda_{sss}}{3\omega_s}\zeta_s^J(x)+\sum_{\substack{m=1,\\ m\neq r\neq s}}^{\infty}\left[\frac{-2\omega_s\Lambda_{mss}}{\omega_m^2-4\omega_s^2}\zeta_m^J(x)\right], \tag{52b}$$

$$\hat{\psi}_{rs}^J(x)=\frac{3(\Lambda_{rrs}+\Lambda_{rsr})}{8\omega_r}\zeta_r^J(x)+\frac{3(\Lambda_{srs}+\Lambda_{ssr})}{5\omega_r}\zeta_s^J(x)+\sum_{\substack{m=1,\\ m\neq r\neq s}}^{\infty}\left[\frac{-3\omega_r(\Lambda_{mrs}+\Lambda_{msr})}{\omega_m^2-9\omega_r^2}\zeta_m^J(x)\right], \tag{52c}$$

$$\hat{\kappa}_{rs}^J(x)=\frac{\Lambda_{rrs}+\Lambda_{rsr}}{4\omega_r}\zeta_r^J(x)-\frac{\Lambda_{srs}+\Lambda_{ssr}}{3\omega_r}\zeta_s^J(x)+\sum_{\substack{m=1,\\ m\neq r\neq s}}^{\infty}\left[\frac{-\omega_r(\Lambda_{mrs}+\Lambda_{msr})}{\omega_m^2-\omega_r^2}\zeta_m^J(x)\right]. \tag{52d}$$

Appendix C

The differentiated dimensional equations of motion for the approximate horizontal/inclined cable model with varying ρ-terms are rewritten as

$$\ddot{u}=(gH/w_C\rho)u''+(EAg/w_C)\left\{\frac{(1+u')N_1+u''N_2}{\rho^4}-\frac{3(1+u')y'y''N_2}{\rho^6}\right\}, \tag{53}$$

$$\ddot{v}=(gH/w_C\rho)v''+(EAg/w_C)\left\{\frac{(y'+v')N_1+(y''+v'')N_2}{\rho^4}-\frac{3(y'+v')y'y''N_2}{\rho^6}\right\}, \tag{54}$$

$$\ddot{w}=(gH/w_C\rho)w''+(EAg/w_C)\left\{\frac{w'N_1+w''N_2}{\rho^4}-\frac{3w'y'y''N_2}{\rho^6}\right\}, \tag{55}$$

where

$$N_1=u''+y'v''+y''v'+u'u''+v'v''+w'w'',$$
$$N_2=u'+y'v'+\frac{1}{2}(u'^2+v'^2+w'^2). \tag{56}$$

Acknowledgements Dr. Narakorn Srinil would like to express his gratitude to the support of the University of Rome 'La Sapienza' Italy, through a *Postdoctoral Research Fellowship*.

References

1. Rega, G.: Non-linear dynamics of suspended cables. Part I: Modeling and analysis. ASME Appl. Mech. Rev. **57**, 443–478 (2004)
2. Rega, G.: Non-linear dynamics of suspended cables. Part II: Deterministic phenomena. ASME Appl. Mech. Rev. **57**, 479–514 (2004)
3. Lacarbonara, W., Rega, G.: Resonant non-linear normal modes. Part II: Activation/orthogonality conditions for shallow structural systems. Int. J. Non-linear Mech. **38**, 873–887 (2003)
4. Nayfeh, A.H.: Nonlinear Interactions: Analytical, Computational and Experimental Methods. Wiley, New York (2000)
5. Rao, G.V., Iyengar, R.N.: Internal resonance and non-linear response of a cable under periodic excitation. J. Sound Vib. **149**, 25–41 (1991)
6. Perkins, N.C.: Modal interactions in the non-linear response of elastic cables under parametric/external excitation. Int. J. Non-Linear Mech. **27**, 233–250 (1992)

7. Lee, C.L., Perkins, N.C.: Non-linear oscillations of suspended cables containing a two-to-one internal resonance. Nonlinear Dyn. **3**, 465–490 (1992)
8. Lee, C.L., Perkins, N.C.: Three-dimensional oscillations of suspended cables involving simultaneous internal resonances. Nonlinear Dyn. **8**, 45–63 (1995)
9. Benedettini, F., Rega, G., Alaggio, R.: Non-linear oscillations of a four-degree-of-freedom model of a suspended cable under multiple internal resonance conditions. J. Sound Vib. **182**, 775–798 (1995)
10. Rega, G., Alaggio, R., Benedettini, F.: Experimental investigation of the non-linear response of a hanging cable. Part I: Local analysis. Nonlinear Dyn. **14**, 89–117 (1997)
11. Rega, G., Lacarbonara, W., Nayfeh, A.H., Chin, C.M.: Multiple resonances in suspended cables: direct versus reduced-order models. Int. J. Non-Linear Mech. **34**, 901–924 (1999)
12. Nayfeh, A.H., Arafat, H.N., Chin, C.M., Lacarbonara, W.: Multimode interactions in suspended cables. J. Vib. Control **8**, 337–387 (2002)
13. Irvine, H.M.: Cable Structures. MIT Press. Cambridge, MA (1981)
14. Srinil, N.: Large-Amplitude Three-Dimensional Dynamic Analysis of Arbitrarily Inclined Sagged Extensible Cables. Ph.D. Dissertation, King Mongkut's University of Technology Thonburi, Bangkok, Thailand (2004)
15. Gattulli, V., Martinelli, L., Perotti, F., Vestroni, F.: Non-linear oscillations of cables under harmonic loading using analytical and finite element models. Comput. Methods Appl. Mech. Eng. **193**, 69–85 (2004)
16. Cai, Y., Chen, S.S.: Dynamics of elastic cable under parametric and external resonances. ASCE J. Eng. Mech. **120**, 1786–1802 (1994)
17. Nielsen, S.R.K., Kirkegaard, P.H.: Super and combinatorial harmonic response of flexible elastic cables with small sag. J. Sound Vib. **251**, 79–102 (2002)
18. Zhao, Y.Y., Wang, L.H., Chen, D.L., Jiang, L.Z.: Non-linear dynamic analysis of the two-dimensional simplified model of an elastic cable. J. Sound Vib. **255**, 43–59 (2002)
19. Zheng, G., Ko, G.M., Ni, Y.Q.: Super-harmonic and internal resonances of a suspended cable with nearly commensurable natural frequencies. Nonlinear Dyn. **30**, 55–70 (2002)
20. Srinil, N., Rega, G., Chucheepsakul, S.: Large amplitude three-dimensional free vibrations of inclined sagged elastic cables. Nonlinear Dyn. **33**, 129–154 (2003)
21. Srinil, N., Rega, G., Chucheepsakul, S.: Three-dimensional non-linear coupling and dynamic tension in the large amplitude free vibrations of arbitrarily sagged cables. J. Sound Vib. **269**, 823–852 (2004)
22. Pakdemirli, M., Nayfeh, S.A., Nayfeh, A.H.: Analysis of one-to-one autoparametric resonance in cables-discretization vs. direct treatment. Nonlinear Dyn. **8**, 65–83 (1995)
23. Lacarbonara, W., Rega, G., Nayfeh, A.H.: Resonant non-linear normal modes. Part I: Analytical treatment for structural one-dimensional systems. Int. J. Non-Linear Mech. **38**, 851–872 (2003)
24. Arafat, H.N., Nayfeh, A.H.: Non-linear responses of suspended cables to primary resonance excitations. J. Sound Vib. **266**, 325–354 (2003)
25. Srinil, N., Rega, G.: Two-to-one resonant multi-modal dynamics of horizontal/inclined cables. Part II: Internal resonance activation, reduced-order models and non-linear normal modes. Nonlinear Dyn. (in press), doi: 10.1007/s11071-006-9087-z.
26. Hagedorn, P., Schafer, B.: On non-linear free vibrations of an elastic cable. Int. J. Non-Linear Mech. **15**, 333–340 (1980)
27. Luongo, A., Rega, G., Vestroni, F.: Monofrequent oscillations of a non-linear model of a suspended cable. J. Sound Vib. **82**, 247–259 (1982)
28. Luongo, A., Rega, G., Vestroni, F.: Planar non-linear free vibrations of an elastic cable. Int. J. Non-linear Mech. **19**, 39–52 (1984)
29. Benedettini, F., Rega, G., Vestroni, F.: Modal coupling in the free nonplanar finite motion of an elastic cable. Meccanica **21**, 38–46 (1986)
30. Takahashi, K., Konishi, Y.: Non-linear vibrations of cables in three dimensions. Part 1: Non-linear free vibrations. J. Sound Vib. **118**, 69–84 (1987)
31. Nayfeh, A.H., Pai, P.F.: Linear and Non-linear Structural Mechanics. Wiley, New York (2004)
32. Gehle, R.W., Masri, S.F.: Active control of shallow, slack cable using the parametric control of end tension. Nonlinear Dyn. **17**, 77–94 (1998)
33. Yu, Z., Xu, Y.L.: Non-linear vibration of cable-damper systems. Part 1: Formulation. J. Sound Vib. **225**, 447–463 (1999)
34. Berlioz, A., Lamarque, C.H.: A non-linear model for the dynamics of an inclined cable. J. Sound Vib. **279**, 619–639 (2005)
35. Wu, Q., Takahashi, K., Nakamura, S.: Formulae for frequencies and modes of in-plane vibrations of small-sag inclined cables. J. Sound Vib. **279**, 1155–1169 (2005)
36. Lacarbonara, W., Camillacci, R.: Non-linear normal modes of structural systems via asymptotic approach. Int. J. Solids Struct. **41**, 5565–5594 (2004)
37. Srinil, N., Rega, G., Chucheepsakul, S.: Non-linear interactions in the 3D free vibrations of horizontal and inclined sagged cables. In: Proceedings of the Fifth International Symposium on Cable Dynamics. Italy, pp. 77–84 (2003)